Forecasting the time of failure of landslides at slope-scale: A literature review

Emanuele Intrieri*, Tommaso Carlà, Giovanni Gigli

Department of Earth Sciences, University of Florence, via La Pira 4, 50121 Florence, Italy.

ABSTRACT

Forecasting the time of failure of landslides at slope-scale is a difficult yet important task that can mitigate the effects of slope failures in terms of both human lives and economic losses. Common applications include public safety situations, where the risk is represented by dwellings built near active landslides or unstable cut slopes that threaten streets and railways, and open-pit mines, for which accurate warnings are fundamental to safeguard workers and simultaneously avoid unnecessary interruptions of the extraction activities.

The scientific literature is populated by many methods, guidelines and approaches regarding forecasting the time of failure or defining the conditions of imminent collapse. Thus, obtaining a synoptic view of the advantages and limitations of these different methodologies has become difficult. At the same time, innovations in technology have opened new possibilities to the application of such techniques, which are examined here.

This paper discusses and classifies these methods, addressing their respective differences and peculiarities to foster the usage even of less popular methods without overlooking the more scientific aspects and issues of landslide forecasting. Finally, an overview of the future trends and challenges is presented to contribute to the debate around this important topic.

1. Introduction

Estimating the risk that is represented by landslides on a global scale is difficult. For instance, damage from landslides is usually attributed to the events that triggered them (as with earthquakes), and small-scale failures are often under-reported (Petley et al., 2005a). The true number of fatalities may be slightly underestimated when victims die of landslide-derived injuries weeks to months following the event (Petley, 2012). Estimates of human loss and economic cost are therefore variable; safe evaluations consider that the average number of annual fatalities is > 4300 per year worldwide (Froude and Petley, 2018). The annual cost in countries such as Italy, the USA and Japan easily exceeds $1 billion (Schuster and Highland, 2001; Klose et al., 2015) and globally is about $19.8 billion, which is about 17% of the average annual global natural disaster losses (Haque et al., 2016); projections that are based on the possible effects of climate change suggest that these numbers will probably increase (Gariano and Guzzetti, 2016).

The United Nations International Strategy for Disaster Reduction (UNISDR, 2006) addresses early warning systems as a powerful tool to reduce risk in a vast range of fields, including landslides. One of the main components of early warning systems is forecasting (DiBiagio and Kjekstad, 2007; Intrieri et al., 2013).

Landslide forecasting consists in the prediction of a slope failure in spatial and/or temporal terms. In the first case the aim is giving a spatial probability of where an instability may occur. This is typically carried out through susceptibility, hazard, or risk maps: the first ones imply classifying, estimating the area or volume, and assessing the spatial distribution of existing and potential landslides in the study area; hazard maps are related to the frequency (i.e. annual probability) of landslides; risk maps also assess the potential damage to the elements at risk (Fell et al., 2008). Susceptibility maps are usually the result of combining the weighted influence that a number of parameters can have on the landslide predisposition, e.g. slope gradient, lithology, land cover, aspect, drainage characteristics, etc. (Ayalew and Yamagishi, 2005; Van Westen et al., 2008; Bui et al., 2016; Le et al., 2018). Hazard maps typically define the probability of occurrence from information concerning the frequency of past events or from models that compute the factor of safety (Dietrich and Montgomery, 1998; Salciarini et al., 2006; Simoni et al., 2008; Rossi et al., 2013). The spatial prediction can also include where and how the detached material will travel and eventually deposit. This is often calculated with empirical or numerical models (Chen and Lee, 2003; De Joode and Van Steijn, 2003; Rickenmann, 2005; Antolini et al., 2016; McDougall, 2016). The topic of spatial landslide prediction would require a deeper dissertation that

---

* Corresponding author.
  E-mail address: emanuele.intrieri@unifi.it (E. Intrieri).

is not within the scope of this paper.

Our focus, in fact, is on the temporal prediction of landslides, that can be defined as the determination of the time of collapse of a landslide (or part of it) within an acceptable margin of error (where the term "acceptable" is linked to the concept of acceptable risk; Fell, 1994). Temporal prediction can be performed at global/regional scale or at slope-scale; the choice of the scale is usually linked to the choice of the monitored parameters. In fact, different approaches exist to predict the time of failure of landslides, depending on which parameter is adopted to indicate probable imminent failure. Typically, regional scale predictions can only be made using rainfall monitoring and a geomorphological, hydro-meteorological approach, while slope-scale predictions can take advantage of a geotechnical approach relating displacement or other kinds of data to the time of failure. Although forecasting methods employing rainfall data exist also for slope-scale applications, Segoni et al. (2018) found out that only 4.2% of the rainfall-based methods they reviewed was conceived for slope-scale, while most of them were for basin or regional scale (Shieh et al., 2009; Brunetti et al., 2010; Ponziani et al., 2012).

The most common use of precipitation data is to derive rainfall thresholds. These typically take the form of rainfall-intensity thresholds, thresholds that are based on the total event rainfall, event-duration thresholds, event-intensity thresholds, and thresholds that are based on antecedent precipitation (Guzzetti et al., 2007). All these methods rely on the fact that rainfall is a major trigger of slope instability. Their widespread use is related to the possibility of making temporal predictions at the regional scale and our ability to perform relatively accurate weather forecasts (Stähli et al., 2015; Piciullo et al., 2018). On the other hand, if the slope-scale detail is needed, since these approaches adopt an indirect indicator of instability (rainfall), they are more prone to false or missed alarms. Such limitation may not always satisfy the requirements of an acceptable margin of error.

Other forecasting methods can provide slope-scale predictions of the time of failure and exploit acoustic emissions, rockfall frequency, pore-water pressure or different indicators as tell-tale signs that suggest that the slope is experiencing structural damage and may be prone to failure (Jurich and Miller, 1987; Szwedzicki, 2003; Rosser et al., 2007; Vilhelm et al., 2008). Although such parameters may be qualitatively considered during expert evaluations of failure risk, their inclusion within codified early warning systems is not common practice.

Finally, the most reliable (and most commonly used) parameters for forecasting the time of failure at the slope-scale are the slope displacement and its derivatives (velocity and acceleration). These kinematic parameters are directly related with the stability conditions of the moving mass (Lacasse and Nadim, 2008), and modern technology provides plenty of proficient instruments to accurately monitor them in real time (Casagli et al., 2017).

From here on, unless otherwise specified, we will refer to prediction or forecasting only in temporal terms. In particular, this paper focuses on slope-scale methods based on kinematic parameters. Especially at this scale, such approaches are still not frequently adopted in risk-management strategies for civil protection, mainly because of the need for a dedicated and often expensive monitoring system (Iovine et al., 2006; Intrieri et al., 2012), but represent a focal point in the mining industry, where concerns regarding workers' safety and the (unnecessary) interruption of activities justify the cost for cutting-edge monitoring systems; in fact, most of the applications and interesting developments of forecasting methods that are based on slope kinematics are documented in this sector (see Section 2.5 "Applications").

Based on all these considerations, the importance of delving into time-of-failure forecasting is apparent. Nonetheless, a recent work that systematically explains, compares and comments on the main methods, with their respective advantages and limitations, is currently lacking in the scientific literature. Therefore, this paper aims to provide a state-of-the-art review for researchers and risk-management operators alike.

2. Classification of kinematics-based failure-forecasting methods

For our purposes, failure (or rupture) is defined as a complete paroxysmal collapse of the material. Although the described methods have sometimes been successfully applied to a variety of cases such as rock specimens (Mufundirwa et al., 2010; Hao et al., 2016), soil specimens (Petley et al., 2005b; Dok et al., 2011), man-made walls (Carlà et al., 2017b) or volcanic eruptions (Voight, 1988; De la Cruz-Reyna and Reyes-Davila, 2001; Smith and Kilburn, 2010; Boué et al., 2015), these methods are mostly applied to unstable slopes. Thus, landslides are used as the main references, but the same concepts are still valid in other contexts.

The rationale for most time-of-failure predictions is that slopes experience displacements that can be described with a creep curve before rupture (Tavenas and Leroueil, 1981). Creep is deformation that varies with time, occurring at constant, largely plastic stress (i.e., most of the deformation is not recoverable after an initial elastic, recoverable strain). Three stages are traditionally individuated, although some authors explained the second stage for brittle materials as a linear superimposition of the first and third stages or a transition between the two (Main, 2000; Amitrano and Helmstetter, 2006). Nevertheless, according to the classic interpretation, the first stage is primary (or decelerating or transient) creep, with the strain rate decreasing logarithmically, followed by secondary (or steady-state) creep with a constant strain rate, and tertiary (or accelerating) creep with an increasing creep rate, which leads to rupturing (Fig. 1).
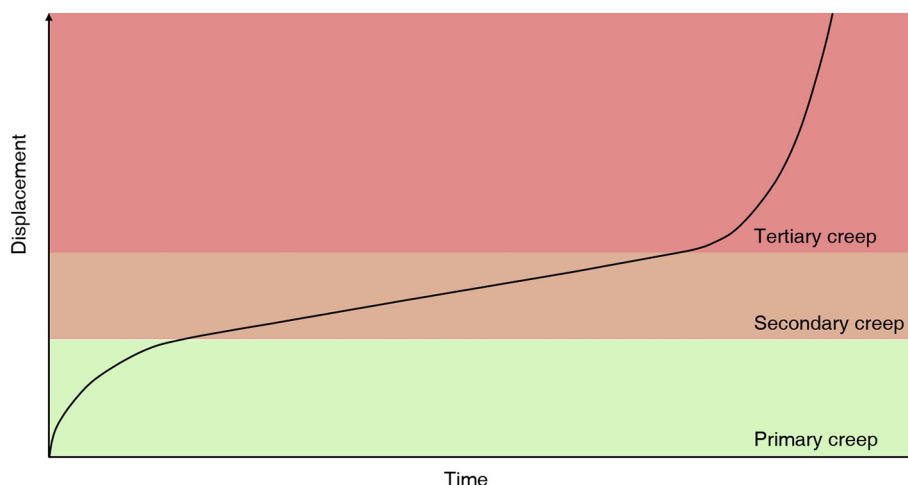

Fig. 1. Conventional three-state interpretation of creep behaviour.

Detailed dissertations regarding creep can be found in Terzaghi (1950), Saito (1969), Zavodni and Broadbent (1978), Varnes (1982), Cruden and Masoumzadeh (1987), Dusseault and Fordham (2008), and Dok et al. (2011).

Time-of-failure prediction methods that are based on kinematic parameters can be classified in two groups:

- Empirical methods: these methods are based on the observation that the displacement velocity critically increases before rupture and usually extrapolate the time of failure through geometrical arguments. Equations are also derived and sometimes described as particular cases of equations that are defined with semi-empirical methods.
- Semi-empirical methods: the starting point of these methods is a general equation that relates the displacement rate to the acceleration, with some empirical constants used.

Typically, the above methods are applied on sliding, toppling and compound landslides, with no intrinsic restrictions to the size, state of activity and type of material (Intrieri and Gigli, 2016). In this paper, examples of rarer applications (rockfalls, wedge failures, slow earth flows) will also be presented.

Other methods are often associated with landslide prediction even though they do not actually provide an estimation of the time of failure:

- Numerical methods: this category encompasses a wide range of methods that analyse and model a time series (for example, decomposing it into several components, often with machine learning) to predict future displacement values based on past observations.
- Methods for the definition of thresholds: this group includes diverse approaches that individuate quantitative signals to suggest a probable failure but cannot provide a time frame for such an occurrence.

Within each group, further classifications would be questionable and not rigorous, so the methods will be described in a broad chronological order and grouped together based on similarity.

2.1. Empirical methods

Without considering the very first attempts at time-of-failure prediction in the literature (Heim, 1932; Jäggli, 1928; Eberhardt et al., 2008; Bonnard, 2006; Federico et al., 2015), the first notable approach regarding failure forecasting was developed by Saito and Uezawa (1961), who introduced a method to forecast the remaining time to slope failure from the secondary creep curve (Saito and Uezawa, 1961; Saito, 1965) or, more successfully, from the tertiary creep curve (Saito, 1969).

Saito and Uezawa (1961) proposed an empirical formula based on the relationship between the constant strain rate $\dot{\varepsilon}$ (expressed in 10^{-4} min) and the time left to failure or life expectancy t_L (expressed in minutes) Eq. (1); t_L is related to the time of failure (t_f) by the relation $t_f = t_L + t_i$, with t_i = time of prediction.

$$log_{10}\ t_L = 2.33 - 0.916 \log_{10} \dot{\varepsilon} \pm 0.59 \tag{1}$$

The reason why the strain rate was used instead of the displacement was because of the limitations that were inherent to the available monitoring instruments at the time.

On the other hand, Saito (1969) developed an empirical, graphical method based on the tertiary creep curve (Fig. 2). According to this method, three points, specifically, $A_1(\Delta D_1, t_1)$, $A_2(\Delta D_2, t_2)$, and $A_3(\Delta D_3, t_3)$, are selected to have an equal difference of displacement ΔD (that is, they must be equally spaced on the Y axis). A_1' and A_3' are projections of A_1 and A_3, respectively, on a line that passes through A_2 and is parallel to the time axis. M and N are the midpoints of $A_1'A_2$ and $A_1'A_3'$, respectively. Then, the time of failure t_f can be obtained as the abscissa of the intersection of a straight line that passes through A_1' and N' with

a straight line that passes through M' and is parallel to the time axis. This procedure was justified through geometrical arguments.

Although Saito recommended a graphical approach, the advent of calculation sheets and algorithms has since made corresponding numerical solutions more practical Eq. (2).

$$t_f = \frac{t_2^2 - t_1 t_3}{2t_2 - (t_1 + t_3)} \tag{2}$$

Hayashi et al. (1988) derived an equation to predict failure at an early stage of tertiary creep (that is, earlier than most other methods, which work better when applied during the latest stage), based on the observation that a higher initial velocity at the beginning of the tertiary creep indicates a closer time to failure Eq. (3).

$$t_L = c(\Delta t)^m \tag{3}$$

where c and m are constants whose values (2.13 and 1.6, respectively) have been empirically calculated from seven natural slope failures, and Δt is the required time interval for a displacement of 10 cm starting from the beginning of the tertiary creep. This procedure has never been popular, and how much the values for c and m can vary is not known without extensive application to other case histories. The main feature of this method is its nominal ability to perform early predictions, although this feature means that forecasts cannot be updated in case of trend changes and the monitoring data must be sufficiently long to catch the beginning of tertiary creep.

Fukuzono (1985a, 1985b, 1990) further developed Saito's idea by proposing a simpler graphical method, which is by far the most used and simple approach to find a slope's time of failure.

This method is valid for tertiary creep, after that the landslide undergoes acceleration at the time t_0 (onset of acceleration). At this point, two possible outcomes can occur (showed in Fig. 3):

a) the velocity (v) increases asymptotically until the landslide collapses at the time t_f, when the velocity is theoretically $v \to \infty$;
b) after an initial acceleration, the velocity decreases and the landslide reaches another equilibrium state without collapsing.

Fukuzono (1985a) calculated that the inverse velocity ($1/v$ or Λ) corresponds to the following in cases of slow and continuous deformation under a constant load until failure Eq. (4):

$$\Lambda \equiv 1/v = [A\ (\alpha-1)]^{1/(\alpha-1)}\ (t_f - t)^{1/(\alpha-1)} \tag{4}$$

where A and α are two values that are found empirically; recent studies revealed that A and α are not independent from each other, varying with the over-consolidation ratio and the type of material (Minamitani, 2007; Dok et al., 2011). Eq. (4) is derived from the linear correlation between the logarithm of acceleration and the logarithm of velocity during tertiary creep, as found by Fukuzono and Terashima (1982) and Fukuzono (1984).

The graphical method that was described by Fukuzono (1985a) consists of plotting the inverse of the velocity versus time Eq. (4). As long as the landslide is at equilibrium, the plot displays a line that is parallel to the time axis; when the velocity asymptotically increases, the plot displays a line whose extrapolation intersects the time axis ($1/v \to 0$) when $v \to \infty$. The time that corresponds to the extrapolated intersection indicates the time of failure. If $\alpha = 2$, the plot is linear and the time of failure equals the predicted time from Saito's (1969) method. In this case, a linear regression is used for the extrapolation.

When $\alpha > 2$ or $1 < \alpha < 2$, the inverse velocity curve is convex or concave, respectively, therefore Fukuzono (1985a) suggested a different graphical method instead of the linear regression (Fig. 4). This approach is rarely used because α typically does not differ much from 2 and the simplification of a linear fit is preferred, provided that it is updated on an ongoing basis to identify the onset of trend changes (Rose and Hungr, 2007). This method consists of drawing a tangent line
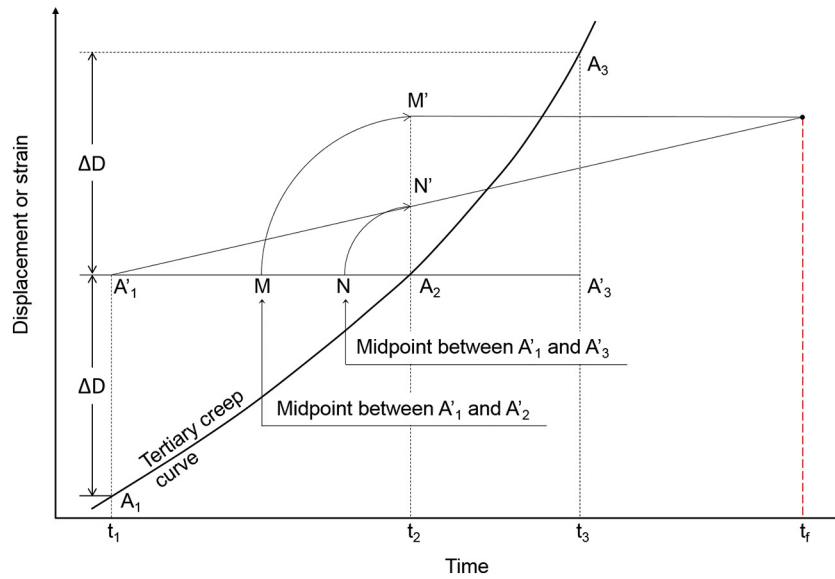
Fig. 2. Graphical approach for determining the time of failure in the tertiary creep range (modified after Saito, 1969).
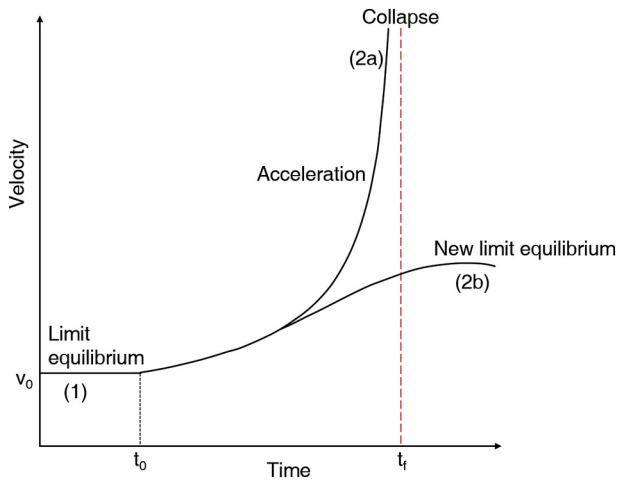

Fig. 3. Kinematic evolution of a landslide; after a period of relative stability that is characterized by constant velocity v_0 during secondary creep (1), if tertiary creep begins, the landslide either accelerates until collapse (2a) or accelerates and then reaches a new equilibrium (2b).
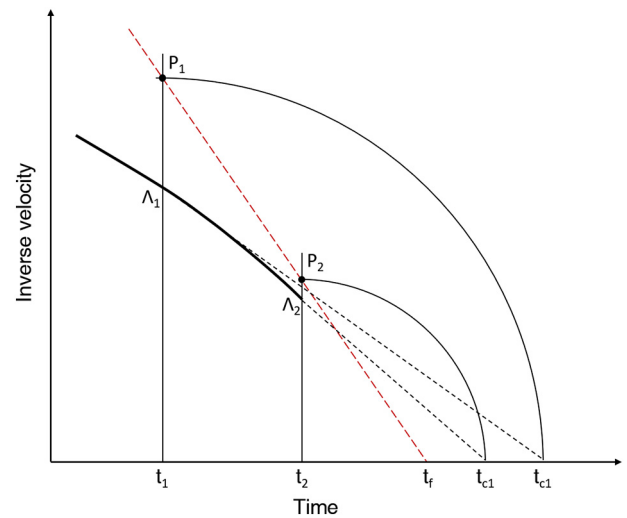

Fig. 4. Graphical method for determining the time of failure when $\alpha \neq 2$ (modified after Fukuzono, 1985a).

to the curve at an arbitrary point Λ_1 that corresponds to time t_1. The tangent crosses the horizontal axis at point t_{c1}. Then, the point P_1 is plotted vertically above Λ_1 so that the segment $t_1\Lambda_1$ equals the segment t_1t_{c1}. This procedure is repeated for another point Λ_2. The abscissa of t_f at which a straight line connecting P1 and P2 crosses the horizontal axis is the time of failure.

Petley et al. (2002) and Petley (2004) related the presence of a linear trend ($\alpha = 2$) to brittle behaviour that was associated with crack formation and first-time failures. On the other hand, Intrieri and Gigli (2016) provided examples of concave-shaped inverse velocity plots that were attributable to first-time failures in brittle materials and linear trends to reactivated landslides (i.e. landslides where the movement occurs along the same sliding surface where it already occurred in the past). De la Cruz-Reyna and Reyes-Davila (2001) applied a visco-elastic material model to the artificial landslides (5 m-high scaled models built in a laboratory) that were studied by Fukuzono (1985a), and concluded that the inverse velocity at the time when the load conditions change cannot be a straight line when the initial stage corresponds to increasing stress (for example, caused by rainfall) and the final stage corresponds to constant stress (for example, because the soil has

reached saturation).

Fukuzono (1985a) applied his method for artificial landslides in loam or sand on slopes that were characterized by different angles and shape. Notably, the failures were triggered by artificial rainfall; although this setup did not comply with the requirement of a lack of external factors (condition necessary for a theoretical creep curve), the predictions were still correct.

In the mining industry, the graphical method that assumes $\alpha = 2$ is often integrated within the trigger action response plan (TARP; Read and Stacey, 2009; Dick et al., 2015) because of its immediate visual feedback. For this reason, the mathematical solution for $\alpha = 2$ that was provided in Fukuzono (1985a) is seldom employed Eq. (5).

$$t_f = \frac{t_2\,(\Lambda_1) - t_1\,(\Lambda_2)}{\Lambda_1 - \Lambda_2} \tag{5}$$

Because of the popularity of Fukuzono's (1985a) method, several authors provided suggestions and guidelines for proficient usage.

This method relies on the inverse value of a derivative parameter (velocity), so the time series experience a high degree of variability, and instrumental or natural noise in displacement measurements

propagates when calculating the inverse velocity. For this reason, Carlà et al. (2017b) recommend performing moving averages to the velocity values (v_t), testing with different values for the number of samples (n) Eq. (6).

$$\overline{v_t} = \frac{v_t + v_{t-1} + \ldots + v_{t-(n-1)}}{n} \tag{6}$$

To address the variability of predictions from noise, Carlà et al. (2017b) suggested using two different moving averages in parallel, each with a higher (long-term moving average, LMA) or lower (short-term moving average, SMA) value of n. Simultaneously projecting the best-fits of both averaged time series will yield two diverse t_f values, with the difference between $t_{f(LMA)}$ and $t_{f(SMA)}$ being indicated as Δ; here, assuming $t_{f(SMA)} < t_{f(LMA)}$, t_{fw} is determined to be between the following range Eq. (7):

$$\left[t_{f(SMA)} - \frac{\Delta}{2}; t_{f(LMA)} + \frac{\Delta}{2} \right] \tag{7}$$

This equation permits us to define a failure window that represents the time frame during which the occurrence of the collapse event is considered most probable.

According to Rose and Hungr (2007), the inverse velocity method is not suitable for predictions over a long period, which should be constantly updated to assess the significance of apparent trend changes. On the other hand, Intrieri and Gigli (2016) suggested reiterating the predictions and considering the entire dataset of forecasted times of failure instead of focusing only on the most recent times. These authors applied this procedure to the methods of Saito (1969), Fukuzono (1985a) and Mufundirwa et al. (2010) and discovered that the most recent displacement monitoring data increase the confidence when estimating the time of failure, but do not necessarily provide more accurate predictions than the older data (provided that predictions are started after the initiation of tertiary creep). In fact, if ongoing predictions are plotted against the time when such predictions are made (prediction plots), the latest forecasts usually either over- or under-predict the time of failure, after a period during which the forecasts oscillate around this time (Sornette et al., 2004; Venter et al., 2013; Intrieri and Gigli, 2016). Therefore, an averaged value of the entire series of forecasts (eliminating outliers and unreasonable values) can provide better results than only the latest predictions.

Starting from the same theoretical basis as Saito and Fukuzono, Azimi et al. (1988) proposed another graphical method (Fig. 5) that was developed from Asaoka (1978), who proposed this approach to assess the final settlement in an edometric test. This method consists of plotting displacements versus time and individuating segments of equal displacement (ΔD). As the velocity increases, these segments will be subtended by increasingly shorter time intervals Δt until $\Delta t \rightarrow 0$

(Fig. 5a). Thus, the final and initial instants of this time interval (t_i and t_{i-1}, respectively) tend to be equal. By plotting t_i versus t_{i-1} during the tertiary creep, data will be roughly aligned on a straight line. The time of failure coincides with the t_i that corresponds with the intercept of this line with the line that represents the identity ($t_i = t_{i-1}$) (Fig. 5b). The extrapolation of this line can enable a timely forecast. Azimi et al. (1988) stressed the importance of choosing only the most recent data because older data may increase the error in the prediction. This method coincides with Fukuzono's (1985a) when $\alpha = 2$, but no applications are found in the literature because of its more complicated implementation.

Li et al. (1996) derived an inverse Verhulst function to predict the time of failure of two landslides Eq. (8):

$$D = \frac{1}{m} \ln \frac{(m - nt_0)t}{(m - nt)t_0} + n_0 \tag{8}$$

where failure is expected to occur for displacement $D \rightarrow \infty$, with m and n corresponding to parameters that represent the best fit of the monitoring data.

More recently, Mufundirwa et al. (2010) continued the tradition of Japanese scholars researching in this field and developed a completely new method "with minimal sensitivity to different lithology, sizes/volumes of failure and more importantly to failure mechanisms". These authors started from Eq. (9), which was first proposed by Fukui and Okubo (1997) and represents strain divergence in the terminal phase of creep failure in rocks.

$$\varepsilon = -B \, log \, (t_f - t) + C \tag{9}$$

where ε is the strain, and B and C are constants. Then, these authors replaced the strain ε with the displacement D and differentiated Eq. (9) with respect to the time t, to obtain the following Eq. (10):

$$\frac{dD}{dt} = \frac{B}{t_f - t} \tag{10}$$

where the left side of Eq. (10) represents the velocity. By multiplying both sides of Eq. (10) by the life expectancy $t_f - t$, the following Eq. (11) is finally obtained.

$$tv = t_f v - B \tag{11}$$

This equation is a straight line, where the product between time and velocity (tv) is the dependent variable (y), v is the independent variable (x), B is the intercept and t_f is the angular coefficient of the line. Therefore, we must plot the velocity data (x) versus the velocity times t (y) and calculate the angular coefficient of the resulting line (Fig. 6) to predict the time of failure; for this reason, this method was termed by the authors as "SLO" (from "slope").

Eq. (11) can be rewritten as a function of t_f as follows Eq. (12):
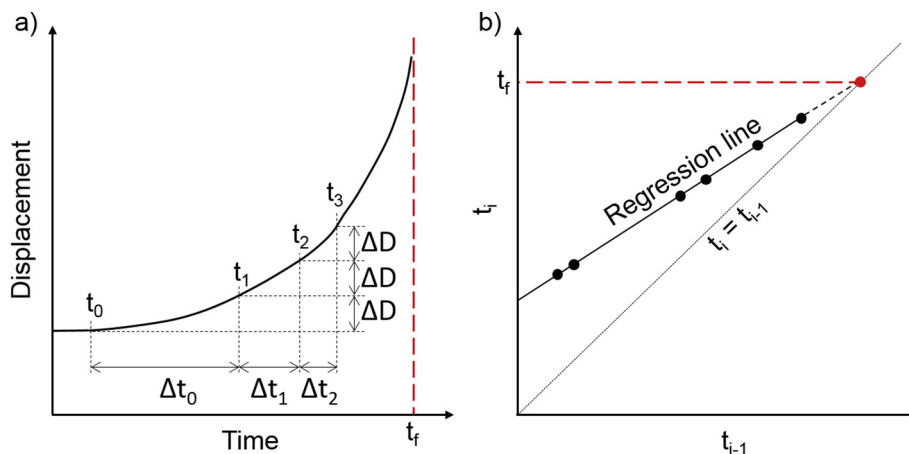

Fig. 5. a: Displacement curves of the final stages before rupture; b: variations in t_i with respect to t_{i-1} (modified after Azimi et al., 1988).
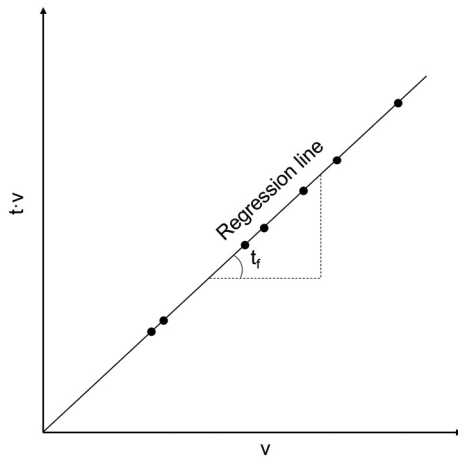
Fig. 6. Plot for predicting failure with the SLO method (modified after Mufundirwa et al., 2010).

$$t_f = t + \frac{B}{v} \qquad (12)$$

Mufundirwa et al. (2010) showed that their method provided reliable predictions where structural failure (rupture plane) was dominant. These results were more conservative than those from Fukuzono's method. Like Fukuzono's approach, also the method developed by Mufundirwa et al. appears to be scale-independent.

Zavodni and Broadbent (1978) developed another method when studying the Liberty Pit slope failure, which showed that data in a log (velocity)-time plot were aligned on a straight line. The ratio between the slope velocity at the middle point between the onset of acceleration and the failure (v_{mp}) and the velocity at the onset of acceleration (v_{OOA}) produced a constant (K). The same ratio was calculated for five other slope failures, producing an average K value of 7.21 with a standard deviation of 2.11 Eq. (13).

$$K = \frac{v_{mp}}{v_{OOA}} \qquad (13)$$

From Eq. (13), the following Eq. (14) could be derived according to the semi-log relationship between the time and velocity.

$$v_f = K^2 v_{OOA} \qquad (14)$$

where v_f is the velocity at failure. The time of failure can then be determined by extrapolating the log(velocity)-time line until v_f is reached.

This method is simple but has two major drawbacks. First, a statistically significant validation is necessary to assess the range of variations in K. Because K is raised to the power of 2, a slight variation in its value can determine critical differences in the calculation of v_f. Second, the on-time recognition and precise determination of the onset of acceleration becomes decisive.

2.2. Semi-empirical methods

The stages that precede failure represent the progressive degradation of a material and, during these stages, parameters such as the displacement may display a rate of growth that follows a common pattern, as shown above. This can represent an underlying physical law that, if completely understood, could provide a theoretical model to exactly link such parameters to the failure. At present, no knowledge exists regarding how to physically describe the process that leads to failure; in fact, the constitutive relationships that are typically used in numerical modelling to assess slope stability solve for the stress, strain and displacement but not the time (Eberhardt, 2008). Therefore, the only option, apart from the phenomenological black-box models that were described in the previous section, is to rely on semi-empirical

approaches.

The method by Voight (1988, 1989a, 1989b), which is a mathematical generalization of Fukuzono's solution, represents the best attempt to provide a law of general validity for this purpose Eq. (15).

$$\ddot{\Omega} = A\,\dot{\Omega}^\alpha \qquad (15)$$

where α and A are empirical constants and Ω indicates any measurable quantity that appropriately describes the phenomenon. The latter can be interpreted in terms of geodetic observations (such as length changes, fault slip, strain, angular changes, or the number of fracturing events), seismic quantities (such as the square root of the cumulative energy release, also called the Benioff strain) or geochemical observations (such as gas-emission rates or chemical ratios) (Voight, 1988). $\dot{\Omega}$ (or $d\Omega/dt$) and $\ddot{\Omega}$ (or $d^2\Omega/dt^2$) represent the "velocity" and "acceleration" of Ω, respectively.

This equation has been successfully applied with hindsight to determine the eruption time of Mt. St. Helens in 1982 (Voight, 1988) by using different parameters, and is reportedly valid for many different materials other than rocks and soils, such as ice, metals, alloys, concrete and polymers.

Voight assumed that failure occurs when $\dot{\Omega}$ reaches an estimated threshold value $\dot{\Omega}_f$, whereas Fukuzono considered this value to be infinite; therefore, the predicted time to failure when using Voight's equation is more conservative. A method to estimate this threshold for large rockslides was proposed by Crosta & Agliardi (2002).

Considering $\dot{\Omega}_f = \infty$ under Fukuzono's (1985a) assumption, Eq. (15), which is expressed in terms of t_f, becomes the following Eq. (16):

$$t_f = \left[\frac{\dot{\Omega}^{(1-\alpha)} - \dot{\Omega}_f^{(1-\alpha)}}{A(\alpha - 1)} \right] + t \qquad (16)$$

Voight's solution is only usable when the data are characterized by continuous acceleration and constant external conditions. In fact, the model fails, or becomes less accurate, when the external conditions are not time invariant, and deviations that are induced by variations in temperature and rainfall regimes occur (Crosta & Agliardi, 2002). To extend analyses to deformation under increasing stress, Kilburn (2012) proposed the following Eq. (17) and tested it on pre-eruptive data from Hawaii.

$$\dot{\Omega} = k(t_f - t)^{-\beta} \qquad (17)$$

where $k = [A(\alpha - 1)]^{1/(1-\alpha)}$ and $\beta = 1/(\alpha - 1)$.

The major drawback of Eqs. (15) and (17) is represented by the necessity of determining two empirical constants α and A. These constants are the same as those in Fukuzono's method, but no graphical solution can be applied in this case. Although Voight's method is often regarded as furnishing the mathematical background of Fukuzono's method, it is rarely applied to real landslide-emergency cases.

Several authors provided experimental values for such constants (Table 1); in particular, A spans over 4 orders of magnitude. Segalini et al. (2018), who studied 26 different pre-failure landslide time series, found that A tends to assume particularly high or low values as α diverges from 2. While α shows moderate variation (roughly between 1 and 3 but is usually close to 2), this characteristic can be sufficient to sensibly affect the results of a prediction. Furthermore, more recent studies of eruption precursors suggested that α is not constant with time but increases from ≈ 1 to ≈ 2 as fracturing progresses (Cornelius and Voight, 1995; Kilburn and Voight, 1998; Kilburn, 2003; Smith et al., 2009; Bell and Kilburn, 2012).

To solve this issue, α is often assumed to equal 2, thus simplifying Eq. (15) into the following Eq. (18) (Lavallée et al., 2008).

$$\frac{1}{\dot{\Omega}} = A(t_f - t) \qquad (18)$$

Alternatively, Hao et al. (2016; 2017) proposed an interesting solution Eq. (19) from Eq. (15), with the additional value of providing a

Table 1
Empirical values for the parameters α and A from different authors; the values marked with an asterisk have been calculated by Segalini et al. (2018) starting from the data published in the corresponding paper indicated in the "references" column. References are listed in alphabetical order.

A	α	Event	References
0.0205*	1.96*	Delabole quarry landslide	Boyd et al., 1973
0.3944	1.4166	Landslide on cut slope	Bozzano et al., 2014
0.1062	1.8059	Landslide on cut slope	Bozzano et al., 2014
0.0994	1.4209	Landslide on cut slope	Bozzano et al., 2014
2.7188	1.2323	Landslide on cut slope	Bozzano et al., 2014
58.4589	0.6217	Landslide on cut slope covered with spritz beton	Bozzano et al., 2014
43.7721	0.7321	Landslide on cut slope covered with spritz beton	Bozzano et al., 2014
66.6634	0.9204	Landslide on cut slope covered with spritz beton	Bozzano et al., 2014
20.9233	0.9064	Landslide on cut slope covered with spritz beton	Bozzano et al., 2014
2.6756	1.1491	Landslide on cut slope covered with spritz beton	Bozzano et al., 2014
0.0024*	1.97*	Hogarth pit landslide	Brawner and Stacey, 1979
0.0191*	2.00*	Nevis Bluff landslide	Brown et al., 1980
0.102	1.994	Mount Beni landslide	Carlà et al., 2017b
–	1.47–2.42	–	Cornelius and Scott, 1993
–	≈1.5	–	Cornelius and Voight, 1995
1–1310.345	1.63–2.59	–	Dok et al., 2011
–	1.5–2.2	–	Fukuzono, 1985a
0.0024*	2.03*	Preonzo landslide	Geopraevent, 2012
0.0016*	1.94*	Afton mine landslide	Glastonbury and Fell, 2002
0.0343*	2.07*	Tuckabianna West landslide	Glastonbury and Fell, 2002
–	2.96	Test by monotonically increasing the boundary displacement	Hao et al., 2013
–	2.5	Creep-relaxation tests	Hao et al., 2014
–	3.0	Fibre-bundle models loaded by increasing stress	Hao et al., 2016
–	2.0	–	Heap et al., 2011
0.0777*	1.93*	Maoxian landslide	Intrieri et al., 2018a
0.0779*	1.96*	Cavallerizzo di Cerzeto landslide	Iovine et al., 2006
0.0008*	2.00*	Xintan landslide	Keqiang and Sijing, 2006
–	≈2.0	–	Kilburn and Petley, 2003
0.1371*	2.05*	Town of Peace River landslide	Kim et al., 2010
0.0109*	2.00*	Huanglongxi landslide	Li et al., 2012
0.0135*	1.77*	La Saxe landslide	Manconi and Giordan, 2016
$(\alpha - 1.814)/0.1781$	1.85–2.46	–	Minamitani, 2007
0.0767*	1.94*	La Chenaula landslide	Noverraz and Bonnard, 1992
0.1570*	2.03*	Selborne landslide	Petley, 2004
0.0119*	2.00*	Betze Post SE landslide	Rose and Hungr, 2007
0.0173*	2.01*	Betze Post SW landslide	Rose and Hungr, 2007
0.0106*	1.94*	Puigcercòs	Royán et al., 2015
0.0056*	1.96*	Asamushi landslide	Saito, 1969
0.0098*	2.01*	Dosan landslide	Saito, 1969
0.2813*	1.85*	Ooigawa	Saito, 1969
0.0548*	1.53*	Braced-up cliff landslide	Schumm and Chorley, 1964
–	3.3	Mount Pinatubo eruption	Smith and Kilburn, 2010
–	2.1	Mount Pinatubo eruption	Smith and Kilburn, 2010
0.0319*	1.97*	Vajont landslide	Sornette et al., 2004
0.0400*	1.90*	Ohto landslide	Suwa et al., 2010
0.0038*	2.15*	Bomba landslide	Urciuoli and Picarelli, 2008
80	1.6	Bezymianny eruption (cumulative seismic strain release)	Voight, 1988
–	1.0	Vajont landslide (3 years before failure)	Voight, 1988
0.037	2	Vajont landslide (near failure)	Voight, 1988
0.1	1.4	Mt. St. Helens (fault movement)	Voight, 1988
0.059	1.96	Mt. St. Helens (line length change)	Voight, 1988
0.002	≈2.0	Mt. St. Helens (tilt)	Voight, 1988
–	1–3	–	Voight, 1989a
–	1.74–2.1	–	Voight, 1989b
0.0004*	2.10*	Chuquicamata open-pit mine landslide	Voight and Kennedy, 1979
–	1.70–2.13	–	Yoshida and Yachi, 1984

graphical solution similar to Fukuzono's method (Fig. 7).

$$\dot{\Omega}\ddot{\Omega}^{-1} = (\alpha - 1)(t_f - t) \qquad (19)$$

This equation is also a straight line. By plotting $\dot{\Omega}\ddot{\Omega}^{-1}$ against t and extrapolating the trend line, its intercept with the time axis provides t_f. So far, this method has only been applied to rock-specimen tests and volcanic eruptions, but no theoretical constraints for successful applications to landslides exist either. Moreover, this equation bypasses the need for knowing the values of the constants in advance and implements a well-known graphical approach, making this method a promising tool for failure forecasting.

2.3. Numerical methods

Numerical methods are used to describe the behaviour of a landslide through mathematical and/or statistical arguments. Rather than forecasting the time of failure, the aim is to predict a landslide's future displacements, often taking advantage of machine-learning models. The basic idea is that measured displacements can be compared to displacements that are simulated by a reference model to confirm that the slope is responding as initially predicted (Newcomen and Dick, 2015). This approach is typically explicated by assessing whether the newly acquired deformation data comply with a pre-determined confidence interval of the predicted displacement. This analysis methodology is usually challenging and finds application only for the specific landslide
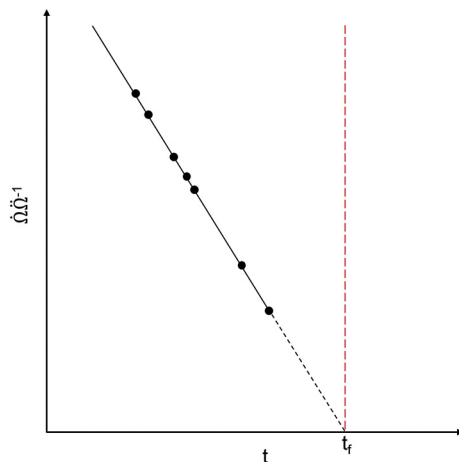
Fig. 7. Graphical method to determine the time of failure (dashed line) in a granite specimen. The prediction is the time that corresponds to the intercept of the trend line (in red) and the time axis (modified after Hao et al., 2017). (For interpretation of the references to colour in this figure legend, the reader is referred to the web version of this article.)

for which it has been calibrated. Numerical methods may be considered particularly suitable to landslides that experience periodic variations in the displacement rate. Nonetheless, this field has experienced a great pulse of research development in the very recent past, even to the point that the literature seems to be quite redundant and not conclusive. Models can also include variables such as the groundwater level, pore pressure, or rainfall intensity–duration. A few such examples are hereby cited.

Chousianitis et al. (2014) introduced an empirical estimator of co-seismic landslide displacements based on Newmark's sliding block model. This topic was also addressed by Du and Wang (2016), who formulated a one-step Newmark displacement model to estimate earthquake-induced slope displacement based on four seismological parameters.

Liu et al. (2014) presented a comparative study on landslide non-linear displacement prediction by means of computational-intelligence techniques. Specifically, these authors evaluated the ability of the support vector machine, relevance vector machine, and Gaussian process theories to fit and predict nonlinear displacements of the Baishuihe landslide in China and the Super-Sauze landslide in the French Alps. Also Miao et al. (2018) proposed a support vector regression (SVR) algorithm to model three pre-defined terms (trend, periodic, and random) of the Baishuihe landslide. In the same area, Zhou et al. (2016) had previously described a particle swarm optimization (PSO; Eberhart and Kennedy, 1995) and support vector machine coupling model to represent the relationship between the rainfall/reservoir level and the displacement of the Bazimen landslide. Similarly, Zhou et al. (2018) used PSO to optimize the parameters of a kernel extreme learning machine (KELM; Huang et al., 2012) to improve predictions (PSO-KELM). Du et al. (2013) adopted a back-propagation neural-network model with selected rainfall–water level factors to predict the displacements of active colluvial landslides in the Three Gorges Reservoir in China. Yao et al. (2015) argued that the applicability of static models such as feed-forward neural networks is quite limited in landslide-prediction tasks and therefore proposed the use of recurrent neural networks that were trained into dynamic predictors of landslide displacement. Krkač et al. (2017) presented a methodology to predict landslide movements with a machine-learning algorithm based on regression trees, which was calibrated to two years of monitoring data of landslide movement, groundwater levels, and precipitation at the slowly moving Kostanjek landslide in Croatia; the displacements were successfully predicted for periods of up to 30 days.

Another exploited field is the use of displacement data to train and

test neural networks. For example, Neaupane and Achet (2004) developed a back-propagation neural network (BPNN) model to predict ground movements at a landslide site in Nepal, which was trained on input variables that typically control the stability of a slope (such as permeability, steepness, and soil-strength parameters). Chen and Zeng (2012) proposed an improved BPNN to consider the nonlinear components that are inherent to a trend of landslide displacement. On the other hand, Gao and Feng (2004) introduced a combined Grey System and Evolutionary Neural Network (ENN) to decompose the monotonously increasing nature of time series of landslide displacements into separate "trend" and "deviation" components.

Corominas et al. (2005) attempted to predict the displacement and velocity of the Vallcebre landslide by solving the momentum equation, in which a viscous term (Bingham and power law) was added. Bernardie et al. (2015) used a combined statistical-mechanical model to predict changes in landslide displacement rates from observed changes in rainfall amounts at the Super-Sauze landslide. Cao et al. (2016) analysed the relationships among the rainfall, reservoir water level, and groundwater according to the step-like displacement behaviour of the Baijiabao landslide and consequently derived an extreme learning machine model for prediction purposes. Lian et al. (2015) proposed a multiple artificial neural network switched-prediction method to identify individual predictors for different environmental factors and thus forecast the displacements of different landslides in the Three Gorges Reservoir area (China).

Further examples have been published by Lu and Rosenbaum (2003), Feng et al. (2004), Randall (2007), Li et al. (2012), and others.

The practical usefulness of numerical methods for early warning may be quite limited because an indication of whether and when a failure might occur is not provided. In fact, these methods were mostly formulated based on statistical approximations of historical data, so any significant deviations in the landslide from its previous deformation behaviour (i.e., from the displacement trend that is observed during the calibration of the model) cannot be predicted. The latter aspect has considerable repercussions when landslides quickly transition from a primary or secondary creep stage to a tertiary creep stage, leading to failure. Therefore, these methods' practical purpose lies in the possibility of detecting when the actual displacement exceeds the forecasted values, implying the onset of an unprecedented acceleration (Zhou et al., 2016).

Few authors attempted to propose solutions to fill this gap. Carlà et al. (2016) linked the probability of the failure occurrence of the Stromboli volcano's flank with the amount of measured "anomalous" slope deformation (i.e., the divergence of the observed data from the predicted data). This task was achieved by sequentially performing one-step-ahead displacement forecasts by means of an Auto-Regressive Integrated Moving Average (ARIMA) model and then comparing the actual measurement with the confidence interval of the forecast. These authors determined that the precursory phase to the August 2014 flank eruption was characterized by a significantly larger total amount and rate of anomalous deformation with respect to what was observed during previous periods of high volcanic activity, which ultimately did not lead to this outcome.

2.4. Other methods to define warning thresholds

Despite not delivering time-of-failure predictions, methods that define the critical thresholds of parameters that indicate a change in the stability conditions of a slope can still be considered within the activities of an early warning system, encompassing forecasting in a broad sense (Intrieri et al., 2013).

The threshold approach is generally more conservative because thresholds are typically set safely before a possible failure; consequently, these thresholds are also more prone to false alarms. For this reason, thresholds and time-of-failure forecasting methods are sometimes integrated into the same early warning system (Intrieri et al.,

2012).

In many cases, completely empirical threshold values that are only based on expert judgement and available monitoring records are implemented (Wyllie and Munn, 1979; Zavodni and Broadbent, 1978; MacRae, 1982; Zavodni, 2001; Iovine et al., 2006; Blikra, 2012; Gigli et al., 2014; Lombardi et al., 2017). However, these values are strictly valid for a specific landslide and lack any consolidated approach or premise. Instead, only slope-scale methods that have a degree of exportability, i.e., methods that are based on a robust observational basis or derived from time-of-failure methods, are described in this section.

For example, Crosta and Agliardi (2002) fitted displacement data from the Ruinon rockslide in the Central Alps (Italy) by using Voight's (1988) equation through the application of non-linear estimation techniques. These authors then determined the parameters A and α and computed velocity–time theoretical curves. Consequently, these authors defined velocity-threshold values that theoretically corresponded to 30, 15, and 7 days before failure to activate pre-alert, alert, and emergency states, respectively.

In a similar fashion, Segalini et al. (2018) explained a method to define theoretical velocity curves that are not dependent on the specific case study. After estimating the parameters A and α and calculating theoretical velocity curves through Fukuzono's (1985a),b) equations, these authors normalized the obtained values with respect to the average and standard deviation. As a result, a normalized, dimensionless velocity curve was obtained to set velocity thresholds. A further advantage was that this type of curve proved to depend on α, while the influence of A was negligible.

Brox and Newcomen (2003) studied the issue of slope-stability prediction in open-pit mines, referring to a number of failure mechanisms such as planar, wedge, stepped-path, toppling, rotational/rock mass, and complex or some combination of the above. Rather than describing a method to define thresholds, these authors directly proposed threshold values, which were partially based on suggestions from Zavodni (2001). Such thresholds use the deformation ε, defined as the ratio between the maximum deformation of the highwall and the total height of the highwall, which can be considered a more normalized parameter than the displacement, thus hinting at a higher exportability of the method. These authors individuated three thresholds that corresponded to ε, equalling 0.1% (development of tension cracks), 0.6% (accelerating movement) and 1% (imminent collapse), respectively; then, these values are expressed in the function of the rock-mass quality (described by the RMR, Bieniawski, 1976). A stable area, an unstable area and a transition zone are hence delimited in the space that is defined by ε and the RMR. These authors also discussed how the dependence on the rock-mass quality and the tolerance to strain are different for each failure mechanism but did not implement such differences in the proposed method, which does not consider the type of failure.

Xu et al. (2011) developed an approach based on the observation that the displacement-time curve becomes almost vertical during the last phase of tertiary creep. To identify a general and quantitative criterion, the displacement is normalized by dividing it with respect to the average velocity of the secondary creep. This method produces a plot that, dimensionally, is a time in both axes. The thresholds that were proposed by Xu et al. (2011) are based on the values that are assumed by the tangential angle of the curve of this plot: when the angle is > 45°, the slope enters the tertiary stage; a value of 80° corresponds to a second threshold; eventually, if the tangential angle > 85°, the slope deformation enters a highly accelerated state that is typical of pre-failure conditions.

Another method that uses the normalization of kinematic parameters to determine warning thresholds was described in Carlà et al. (2017c). These authors analysed a dataset of 40 slope failures in coal mines, which was provided by Cabrejo and Harries (2012), and discovered that the ratios of the calculated accelerations over two fixed time ranges before failure were constant for all cases. For example, the ratio between the acceleration over the last 3 h (a_{3h}) and that over the

last 24 h (a_{24h}) before failure was ≈ 7 for all cases. Thus, when the acceleration at any time is seven times greater than the acceleration 21 h earlier, the failure is expected to occur in 3 h. Similarly, the ratios a_{3h}/a_{48h} and a_{24h}/a_{48h} were constant (≈ 13 and ≈ 2, respectively). This approach has direct early warning applications; in fact, by continuously calculating and plotting the value of the acceleration ratio, for example, a_{3h}/a_{24h}, an alarm can be issued when the value of seven is approached, indicating failure in 3 h. This method has been validated for as many as 40 cases, although all of them likely shared similar geological conditions (details regarding the failure mechanism, size, rock-mass quality and other important parameters were not furnished in the database by Cabrejo and Harries, 2012). Therefore, further studies are necessary to understand how the values of these ratios change depending on the context. Otherwise, this method can still prove to be a useful tool, provided that a number of failures, which are needed to calibrate the value of the ratio, have occurred in the same area.

Manconi and Giordan (2016), based on Fukuzono's (1985a) method, developed an approach to increase the confidence of the forecasts. This method consists of applying a linear regression analysis to the inverse velocity. This procedure is repeated for 1000 iterations by applying a bootstrap resampling strategy (Efron, 1979) to derive robust assessments of errors that are associated with the estimated regression coefficients. The model vs. data fitness is then evaluated by calculating both the Pearson's correlation coefficient (CCORR) and the root mean square (RMS) of the residuals of the difference between the data and the model. A failure window is defined between the 5th and 95th percentiles of the bootstrap distribution, while the best-fit model is considered the most probable time of failure. This method enables the user to implement thresholds when the forecast confidence level is sufficiently high (for example, when CCORR > 75%).

Carlà et al. (2017b) also started from Fukuzono's (1985) method and derived two threshold levels. The first is triggered at the onset of acceleration, which is defined as the time when a short-term moving average (SMA) of the displacement time series crosses above a long-term moving average (LMA) (positive cross-over). Such moving averages are generally stronger than those that are designed to simply smooth the inverse velocity plots (as described in Section 2.2). If employed to establish thresholds, the SMA should be set so that it already smooths out most of the smaller fluctuations, while the LMA should be calculated over three or four times the SMA's period. The second threshold that was proposed by Carlà et al. (2017b) is triggered at a time that corresponds to the beginning of the failure window, as defined in Section 2.2. The application of thresholds that are based on failure windows was tested on a landslide retaining wall in Canada (Carlà et al., 2017d).

2.5. Applications

Table 2 lists a series of papers from the literature that adopted the empirical or semi-empirical failure-forecasting methods described herein. The most used was Fukuzono's (1985a), probably because of its fast and easy-to-use approach. A few cases involved volcanic eruptions, which were also included because they shared the same methods (mostly semi-empirical) that are used for landslides.

One of the fields where all these approaches are most frequently used is the mining industry. As noted by Hutchinson (2001), the risk in open-pit mines is potentially very serious in terms of both human lives and economical losses because of continuous extraction activities often compromising slope stability and the high values of the elements at risk, given the continuous presence of personnel and the economic consequences of interrupting work because of collapses or even false alarms that are issued by poor warning procedures. Another reason is that open-pit slopes display optimal rock exposures and are usually monitored by reliable and cutting-edge displacement-monitoring networks. Moreover, the people in charge of the TARP and monitoring systems are also at risk, so any complicated relationships with local

Table 2

Literature examples of applications of empirical and semi-empirical failure-forecasting methods. In the description of the event, the term "landslide" has been used when the specific type of landslide is not defined, is unknown or is too complex to be shortly described. With the term "non-failure" are indicated those movements that, although showing intense phases of deformation typical of the tertiary creep, ultimately did not reach failure.

Reference	Forecasting method	Field of application	Description of the event	Applied before the event
Atzeni et al., 2015	Fukuzono, 1985a	Open-pit mining	1 rockslide in a sandstone quarry	Yes
Azimi et al., 1988	Azimi et al., 1988	Public safety (slope failures), civil engineering	Arvan valley rockslide (in gypsum), 1 retaining wall, Dosan earth flow, Soya earth slide, Vajont landslide	Only in 1 case out of 5 was applied before the event
Carlà et al., 2017a	Fukuzono, 1985a	Open-pit mining	4 planar and 1 toppling failures in rock, 4 non-failures	No
Carlà et al., 2017b	Fukuzono, 1985a	Public safety, (slope failures), civil engineering	Mt. Beni rockslide, Vajont landslide, Volterra medieval city walls, 1 debris talus (Stromboli volcano)	No
Carlà et al., 2018	Fukuzono, 1985a	Open-pit mining	1 rockslide	No
Casagli et al., 2009	Fukuzono, 1985a	Public safety (volcanic eruption)	Stromboli eruption	Yes
Corcoran and Davies, 2018	Fukuzono, 1985a; Voight, 1988	Materials science	3 metal specimens valid for power-station components	No
Cornelius and Voight, 1994	Voight, 1988	Public safety (volcanic eruption)	Redoubt eruption	No
Cruden and Masoumzadeh, 1987	Saito, 1969; Zavodni and Broadbent, 1978	Open-pit mining	Luscar rockslide	No
Fukuzono, 1985a	Fukuzono, 1985a	Research	5 artificial landslides (in loam or sand)	No
Dick et al., 2015	Fukuzono, 1985a; Mufundirwa et al., 2010	Open-pit mining	1 rockslide	No
Dok et al., 2011	Fukuzono, 1985a,Fukuzono, 1985b	Research	25 soil specimens	No
Gigli et al., 2011	Fukuzono, 1985a	Public safety (slope failure)	Montebeni rockslide	Yes
Hao et al., 2017	Hao et al., 2017	Research, public safety (volcanic eruption)	3 granite specimens, Bezymianny eruption, Mt. St. Helens eruption	No
Harries et al., 2006	Empirical threshold	Open-pit mining	Mt. Owen landslide	Yes
Heim, 1932	Not available	Public safety (slope failure)	Linthal rockslide	Yes
Hungr and Kent, 1995	Fukuzono, 1985a	Open-pit mining	Waste-dump failure in coal mine	Yes
Hutchinson, 2001	Fukuzono, 1985a	Public safety (slope failure)	Vajont landslide	No
Intrieri and Gigli, 2016	Saito, 1969; Fukuzono, 1985a; Mufundirwa et al., 2010	Public safety (slope failures and volcanic eruption), open-pit mining	14 landslides, 1 volcanic eruption	No
Intrieri et al., 2018a	Fukuzono, 1985a	Public safety (slope failure)	Xinmo (Maoxian) landslide	No
Iovine et al., 2006	Empirical threshold	Public safety (slope failure)	Cavallerizzo di Cerzeto landslide	Yes
Kayesa, 2006	Empirical threshold	Open-pit mining	Letlhakane rockslide	Yes
Kennedy and Niermeyer, 1970	Not available	Open-pit mining	Chuquicamata rockslide	Yes
Kothari and Momayez, 2018	Fukuzono, 1985a	Open-pit mining	22 landslides	Not available
Krähenbühl, 2006	Fukuzono, 1985a	Public safety (slope failures)	2 rockslides	Yes
Lavallée et al., 2008	Voight, 1988	Public safety (volcanic eruption)	Colima volcano	No
Loew et al., 2017	Empirical threshold; Fukuzono, 1985a	Public safety (slope failure)	Preonzo rockslide	Yes
Manconi and Giordan, 2016	Fukuzono, 1985a	Public safety (slope failure)	Preonzo rockslide	No
Mazzanti et al., 2015	Fukuzono, 1985a	Public safety (slope failures)	La Saxe rockslide	No
Mufundirwa et al., 2010	Mufundirwa et al., 2010	Open-pit mining, public safety (slope failures), research	10 rockslides	No
			Undisclosed rockslide, Asamushi landslide, Vajont landslide, Shikotsu welded-tuff specimen	No
Newcomen and Dick, 2015	Empirical threshold	Open-pit mining	Manefay landslide	Yes
Osasan and Stacey, 2014	Fukuzono, 1985a	Open-pit mining	2 landslides	Yes
Petley, 2004	Fukuzono, 1985a	Research	Artificially triggered rotational slide in clay	No
Petley et al., 2005b	Fukuzono, 1985a	Research	Haney clay specimen	No
Petley et al., 2005c	Fukuzono, 1985a	Public safety (slope failure)	Tessina landslide	No
Rose and Hungr, 2007	Fukuzono, 1985a	Open-pit mining	La Clapiére landslide, Liberty Pit landslide, 3 rockslides at Betze-post, 1 undisclosed landslide	Only in 4 cases out of 6 was applied before the event
Saito, 1965	Saito, 1965	Public safety (slope failures)	1 retaining wall, Dosan earth flow, Soya earth slide, 1 non-failure	Yes
Saito, 1969	Saito, 1969	Public safety (slope failures)	Asamushi landslide, Ooigawa landslide, Dosan landslide	Yes
Saito, 1969	Saito, 1965; Saito, 1969	Public safety (slope failure)	Takabayana landslide	Yes
Säitele et al., 2016	Fukuzono, 1985a	Public safety (slope failure)	Preonzo rockslide	Yes
Suwa, 1991	Saito, 1969	Public safety (slope failure)	Saigo rockslide (in tuff)	Yes
Venter et al., 2013	Fukuzono et al., 1985a; Mufundirwa et al., 2010	Open-pit mining	2 landslides	No
Voight, 1988	Voight, 1988	Public safety (slope failure, volcanic eruptions)	Bezymianny eruption, Mt. St. Helens eruption, Vajont landslide	No
Xu et al., 2011	Xu et al., 2011	Public safety (slope failures), open-pit mining	Jiminsi landslide, Daye landslide, open-pit landslide, Baishi landslide	No

Table 2 (continued)

Reference	Forecasting method	Field of application	Description of the event	Applied before the event
Zvelebil, 1985	Not available	Not available	Decin rockfall in sandstone	Yes
Zvelebil and Moser, 2001	Empirical threshold; Fukuzono, 1985a	Public safety (slope failures)	3 landslides	Yes

authorities and the general public, which usually compound the difficulties that are observed in other emergencies and in the management of an EWS, are absent. Some of these factors also apply to the safety of rail and road routes (such as in Saito, 1969).

Applications with civil-protection and public safety purposes (for example landslides threatening people, buildings, environment, infrastructures) are proportionally rarer (this number grows if back-analyses are counted). The primary reason is probably the common lack of early warning systems that are implemented before failure.

Many of the events listed in Table 2 are rockslides, but this observation is biased by the fact that many applications originate from the open-pit mining industry. Translational and rotational slides and toppling are also documented. Generally (as documented in Intrieri and Gigli, 2016), no restrictions exist regarding the type of material, state of activity (first-time failure or reactivation) and volume of a landslide.

3. Discussion and conclusions

Determining the method with the best performance among the several forecasting methods that were described in this paper is difficult, mainly because many methods do not have enough applications to be properly evaluated and seldom applications involved predictions that were made before the event (see Table 2); furthermore, only few papers made direct comparisons between different methods (Venter et al., 2013; Dick et al., 2015; Intrieri and Gigli, 2016). One of the aims of this paper was to increase the availability of these less common approaches, which could bear new input in this research field.

Many methods imply a graphical solution, which is probably one of the main features by which they should be evaluated; using the words of Lambe (1973), "an outstanding plot can go far towards giving […] perspective and understanding of a process or an event". In this regard, Fukuzono's (1985a) method clearly appears to be the most graphically communicative, although very good forecast representations can be obtained with every method, for example, by plotting the predicted time of failure as a function of the time when the prediction is made.

The fact that Fukuzono's method is the most used does not imply it is the most accurate; this method still exhibits specific drawbacks because it is based on the inverse value of a derivative parameter, so it is strongly affected by noise in the measured displacement and is much more sensitive (i.e., the forecasted time of failure experiences strong fluctuations) when the velocities are small (Carlà et al., 2017a). Similarly, methods that are based on acceleration (Voight, 1988; Hao et al., 2016) also experience a propagation of errors when measuring the displacement, differently from methods (such as in Saito, 1969) that are directly applied on displacements. These issues can be solved but using forecasting methods still presents difficulties. First, appropriate filtering and a degree of experience are frequently required to interpret the confidence of a prediction. Second, the determination of the onset of acceleration (which can be used as the starting time to make reasonable forecasts) is often a problematic task; similarly, detecting when the slope has reached a new equilibrium and tertiary creep acceleration has stopped is also important because all the above forecasting methods assume an accelerating trend, whereas abrupt decelerations can disturb predictions (as shown in the case studies of Mazzanti et al., 2015). Solutions to address these issues have been presented in this paper.

At present, the most reliable approach appears to be employing more than one method (including those to determine thresholds, as described in Section 2.4) and making decisions according to the average or safest prediction.

The experiences that were reported in this paper show that these forecasting methods are based on physical behaviours that are shared among many different environments and that failures can be forecasted for to a variety of phenomena (rockslides, earth slides, walls, eruptions, and specimens), materials (rock, earth, glass, and metal), volumes (from cubic centimetres to millions of cubic metres), geometries (planar failures, wedge failures, curvilinear sliding surface, and toppling) and

parameters (displacement, velocity, acoustic emissions, and seismic or geochemical quantities). Furthermore, contrary to what is often assumed (Voight, 1988; Rose and Hungr, 2007), landslides can also be forecasted when external forces are acting on them, as demonstrated by Intrieri and Gigli (2016), who relaxed this assumption. The full potential of such methods is still to be exploited, and interesting scientific and technological advancements could determine the future trends in this field. Some possibilities are described as follows.

Models and experiments on rock specimens that display brittle creep behaviour have revealed the existence of power-law relationships between the time of failure and the applied stress, where a number of constants that depend on the rock properties and ambient conditions also play a role, including the strength of the rock, temperature, water saturation and chemical-corrosion processes (Charles, 1958; Scholz, 1972; Amitrano and Helmstetter, 2006). Knowledge of all these parameters theoretically allows the user to deterministically calculate the time of failure.

When scaling up to a more complex system (such as a landslide), tertiary creep still typically assumes the shape of a power law (usually with a high exponent, which makes it very similar to an exponential law; Lockner, 1993; Zvelebil and Moser, 2001; Crosta and Agliardi, 2003; Amitrano and Helmstetter, 2006; Cruden and Masoumzadeh, 1987; Dok et al., 2011; Corcoran and Davies, 2018) but calculating the time of failure starting from a landslide's characteristics is currently not possible. As Hutchinson (2001) noted, a degree of uncertainty exists partially because of uncertainties in extrapolating the creep curves and especially because these features may be irregular (non-monotonic, as with case 2b in Fig. 3), for instance, because of changes in the internal or external conditions or simply instrumental noise.

The existence of a power-law relationship between the displacement and time in fracturing (brittle) materials can be attributed to crack propagation (Petley, 2004), particularly to a positive feedback process (Main, 2000; Corcoran and Davies, 2018) where the increasing length of the propagating cracks increases the stress intensity at the tip of the crack itself and, therefore, the velocity of further crack propagation (Atkinson, 1984; Amitrano and Helmstetter, 2006). Such a self-feeding process creates the striking non-linearity of tertiary creep.

However, accelerations that fit a power law can also be observed in cases where fracturing does not occur at all (reactivated landslides or earth flows). This phenomenon was observed in the Marano landslide, an earth flow in central Italy that had an estimated volume of 0.7 million m^3 and experienced periodic reactivations (the last event was in 1996; Bertolini et al., 2004). In 2018, a prolonged period of rainfall caused a new acceleration of the landslide, which was monitored through ground-based interferometric synthetic aperture radar (GB-InSAR) to evaluate the risk of river damming because of the fast progression of the toe.

The GB-InSAR recorded a strong accelerating trend during the morning of 11 March 2018 (Fig. 8). The inverse-velocity method was then implemented to detect a point when the landslide could have experienced a paroxysmal acceleration, leading to a fast obstruction of the river.

The application of Fukuzono's (1985a) method showed a good linear trend ($R^2 = 0.95$) that intercepted the horizontal axis around 11 March at 22:15 (Fig. 8). Although the linear fitting was quite good, a more detailed observation showed a slightly concave trend until 18:00 (as generally observed for this type of landslide; Petley, 2004; Petley et al., 2005b), when the slope of the inverse velocity increased and became more linear. Roughly at the time when the trend line intercepted the horizontal axis, the landslide reached the maximum velocity and continued at a constant rate (around 2.3 m/day as measured along the radar line of sight). The strong peak that was recorded around 21:00 was considered an instrumental effect because it was caused by phase wrapping, which means that the actual velocity at that moment was too high for the capabilities of the system. The absence of any acceleration implies the equilibrium of the forces acting on the landslide, so this

behaviour can be explained with a friction model. On 13 March 2018, the landslide experienced a further smooth deceleration, leading to very low to null displacements (occasionally interrupted by minor re-activations after rainfall).

In such a case, the time of failure must not be interpreted as a proper "failure" or a collapse but still as a paroxysmal event, which consists of an abrupt acceleration that drastically changes the kinematics of an earth flow and can cause severe damage. One experience of how earth flows can evolve paroxysmally can be found in Berti et al. (2013). From the perspective of public safety, such events can be considered identical to collapses.

The existence of a power-law relationship, even without crack propagation, means that a corresponding positive feedback mechanism must also occur also in earth flows. Future research in this topic should also involve shedding light on what this possible process represents and maybe investigate if debris flows can also be forecasted with the same tools. As highlighted by Voight (1988), a power-law relationship with the time of failure is not exclusive to brittle rocks but can be established for a number of parameters and applications (as shown in Table 2).

A similar experience of an earth flow undergoing a catastrophic failure after a long period of ductile deformations was reported by Fletcher et al. (2002). This case involved the Attachie landslide (Canada), which consisted of over-consolidated glaciolacustrine clay and silt. Borehole samples and tests revealed that 31% of the source volume was low-plasticity or non-plastic silt, 48% was plastic clayey silt or clay, and 21% was sand. Clay samples from near the sliding surface contained highly plastic clay with a clay fraction of 60–70% and a plasticity index over 30%. Fletcher et al. (2002) attributed the sudden development of the Attachie landslide into an extremely rapid flow slide of 6.4 million m^3 to three possible causes (where mechanisms 2 and 3 both require the presence of non-plastic material, silt in this case):

1. undrained brittleness from the collapse of a metastable structure: this mechanism is typical of quick (sensitive) clays and liquefiable soils and occurs when a disturbance (e.g., an undrained load) increases the pore-pressure as the unstable clay particle structure collapses (Gregersen, 1981); as Hutchinson (1987) noted, undrained head loading alone can be a cause for otherwise unexpected, rapid displacements.
2. Internal strength of the slide mass: if a failure occurs along a compound surface, the moving mass must be broken up by internal shears to form a kinematically admissible mechanism; if the slide mass retains sufficient brittleness at the moment of the break up, a paroxysmal phase may occur (Hutchinson, 1987).
3. "Macroscopic" brittleness: this mechanism involves the opening of multiple tension cracks because of the slow displacements of the landslide, which are then filled with loose material; if surface water saturates this material, liquefaction and heavy fluid pressure can occur inside the cracks (Hutchinson, 1987).

Future trends in landslide prediction will also be fostered by technological advancements in monitoring techniques. The most striking example is related to recent developments in interferometric satellites. The potential of this technique has long been evident, but only after the launch of satellites with relatively short revisiting times (a few days as opposed to a few weeks) have the first feasibility tests been conducted. In particular, the Sentinel-1 constellation, which has an effective revisiting time of 6 days, is a game-changer in the interferometric monitoring scene. Although proper predictions (i.e., predictions made before the event) are not present in the scientific literature (at the time of writing), promising experiences have shown that a continuous check of satellite data would have permitted scientists to properly forecast deadly events such as the Xinmo landslide (Maoxian, China) in 2017 (Intrieri et al., 2018a), which caused > 100 casualties, and a landslide in an undisclosed copper open-pit mine that killed several workers (Carlà et al., 2018), because both events were anticipated by clear
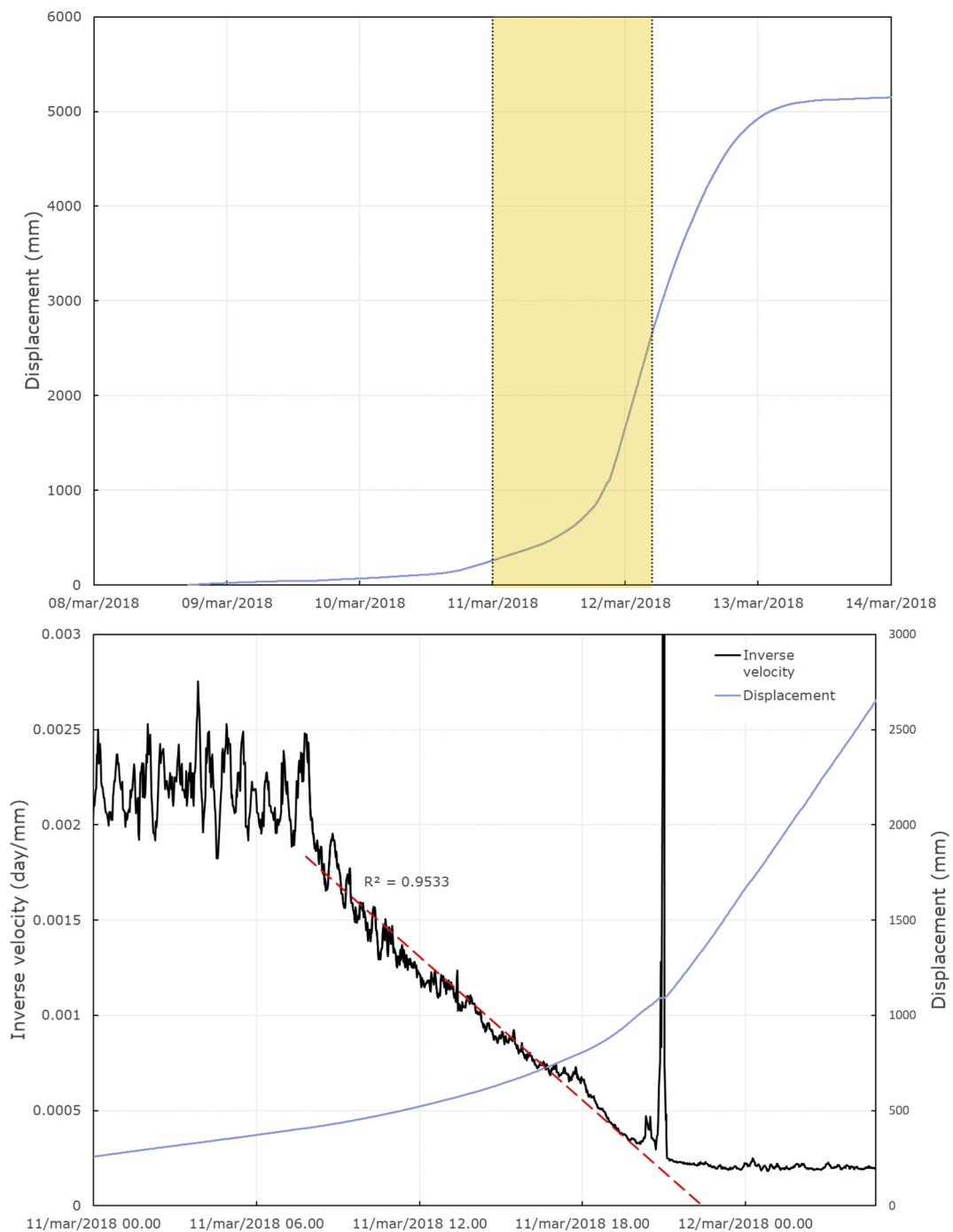
Fig. 8. Top: displacement time series of a portion of the Marano landslide as measured by a GB-InSAR. The yellow rectangle represents the time window zoomed below, in which the inverse velocity is plotted and the red dashed line represents the linear trend. The displacement and inverse velocity values were measured along the line of sight of the instrument. (For interpretation of the references to colour in this figure legend, the reader is referred to the web version of this article.)

tertiary creep.

Appropriate monitoring and early warning programs that exploit satellite data could also be set for public administrations to continuously monitor entire regions by implementing a systematic processing chain of interferometric acquisitions to create continuously updated ground-deformation data. For instance, one application is being tested in the Tuscany Region (Italy) with the Sentinel-1 constellation (Raspini et al., 2018), where displacement time series that are continuously updated with the most recent available acquisitions are analysed to identify points where changes in the kinematics occur.

Even terrestrial instruments are changing what were only recently

considered consolidated assumptions. For example, the capability of modern GB-InSAR apparatuses to monitor areas (not only single points) in a few tens of seconds enables us to further push the limits of what was considered (near) real-time monitoring. Rose and Hungr (2007) and Mufundirwa et al. (2010) argued that very brittle (or more appropriately, rigid) materials would not allow for any warning because sudden collapses cannot be anticipated by any measurable deformation. This assumption was true until recently, when new experiences (Carlà et al., 2017a) showed that even small failures in very good-quality rock masses can show tertiary creep curves, permitting a prediction of the rupture time minutes or tens of minutes in advance. Therefore, the use

of cutting-edge near real-time monitoring instruments sensibly increases the possibility of using forecasting methods.

GB-InSAR also has the advantage of performing measurements over a broad coverage area (instead of on single discrete points). This capability is generally under-used, and the wide dataset that is available is often reduced to a small number of selected points that are used for time-series analyses. For example, a possible approach to exploit GB-InSAR data was provided by Dick et al. (2015), who merged two common practices that have been adopted in open-pit mines worldwide in the framework of an early warning system: Fukuzono's method (Fukuzono, 1985a) and displacement monitoring that is performed through a GB-InSAR. To fully use spatial area data from GB-InSAR, Dick et al. (2015) suggested starting with selecting a single benchmark pixel (either the one that triggered a warning threshold or the one that measured the highest accumulated displacement) and then performing time-of-failure prediction methods over both this pixel and a cluster of adjacent pixels that experienced at least 50% of the displacement of the benchmark.

Despite the relevance of the performances provided by these and similar innovations, the many experiences reported in Table 2 show that in some cases a high precision or a high acquisition frequency were not necessary to forecast the time of failure, e.g. when the landslide has a clear and long tertiary creep phase. Considering the above, a dramatic increase in the diffusion of the practice of time-of-failure forecasting could come along with low-cost instrumentations capable of furnishing displacement data of a reasonable quality. Interesting results could come from the development of Wireless Sensor Networks (WSN) performing ranging measurements using the same ultrawide band signal used to transfer data, thus bypassing the cost related to specific sensors (Intrieri et al., 2018b; Mucchi et al., 2018). Another promising technology for early warning applications is the Radio-Frequency Identification (RFID), that is based on tags that can be installed with a low environmental impact and measure their relative distances with high temporal resolution (Le Breton et al., 2019). Furthermore, in the last years, single-frequency Global Positioning System (GPS) chips available at a lower cost have been used for landslide early warning systems (Benoit et al., 2015). The development of low-cost instruments can therefore enable the monitoring where, for economic reasons, it was not possible or can enable the installation of many measurement points to allow for spatially distributed observations at high spatial resolution, thus reducing the cost for rapid mapping.

Landslide forecasting is a topic that surely deserves more research efforts because of its effects on society. The state of the art of the most relevant studies in this field was defined in this paper to set a starting point for future works. The relationships between the kinematics and time of failure of a slope have been adequately described, but a robust link between geomorphological, geotechnical, and geomechanical features and kinematics (or other parameters acting as collapse indicators) is still missing. New insights could be derived from joint contributions from different research and industry fields, such as engineering geology, materials science, open-pit mining, and remote sensing.

Acknowledgements

Data from the Marano landslide were kindly provided by the Civil Protection of the Emilia Romagna Region and by the National Department of Civil Protection.

References

Amitrano, D., Helmstetter, A., 2006. Brittle creep, damage, and time to failure in rocks. J. Geophys. Res. Solid Earth 111, B11.
Antolini, F., Barla, M., Gigli, G., Giorgetti, A., Intrieri, E., Casagli, N., 2016. Combined finite–discrete numerical modeling of runout of the Torgiovannetto di Assisi rockslide in central Italy. Int. J. Geomech. 16 (6), 04016019.
Asaoka, A., 1978. Observational procedure of settlement prediction. Soils Found. 18 (4), 87–101.

Atkinson, B.K., 1984. Subcritical crack growth in geological materials. J. Geophys. Res. Solid Earth 89, 4077–4114.
Atzeni, C., Barla, M., Pieraccini, M., Antolini, F., 2015. Early warning monitoring of natural and engineered slopes with Ground-based Synthetic-Aperture Radar. Rock Mech. Rock. Eng. 48, 235–246.
Ayalew, L., Yamagishi, H., 2005. The application of GIS-based logistic regression for landslide susceptibility mapping in the Kakuda-Yahiko Mountains, Central Japan. Geomorphology 65 (1–2), 15–31.
Azimi, C., Biarez, J., Desvarreux, P., Keime, F., 1988. Prévision d'éboulement en terrain gypseux. In: Bonnard, C. (Ed.), Proceedings of the 5th International Symposium on Landslides, Lausanne. vol. 1. A.A. Balkema, Rotterdam, pp. 531–536 (In French).
Bell, A.F., Kilburn, C.R.J., 2012. Precursors to dyke-fed eruptions at basaltic volcanoes: Insights from patterns of volcano-tectonic seismicity at Kilauea volcano, Hawaii. Bull. Volcanol. 74 (2), 325–339.
Benoit, L., Briole, P., Martin, O., Thom, C., Malet, J.-P., Ulrich, P., 2015. Monitoring landslide displacements with the Geocube wireless network of low-cost GPS. Eng. Geol. 195, 111–121.
Bernardie, S., Desramaut, N., Malet, J.-P., Gourlay, M., Grandjean, G., 2015. Prediction of changes in landslide rates induced by rainfall. Landslides 12 (3), 481–494.
Berti, M., Corsini, A., Daehne, A., 2013. Comparative analysis of surface roughness algorithms for the identification of active landslides. Geomorphology 182, 1–18.
Bertolini, G., Casagli, N., Ermini, L., Malaguti, C., 2004. Radiocarbon data on Lateglacial and Holocene landslides in the Northern Apennines. Nat. Haz. 31 (3), 645–662.
Bieniawski, Z.T., 1976. Rock mass classification in rock engineering. In: Proceedings of a Symposium on Exploration for Rock Engineering. vol. 12. pp. 97–106.
Blikra, L.H., 2012. The Åknes rockslide. In: Clague, Norway.J.J., Stead, D. (Eds.), Landslides: Types, Mechanisms and Modeling. Cambridge University Press, pp. 323–335.
Bonnard, C., 2006. Technical and human aspects of historic rockslide dammed lakes and landslide dam breaches. Ital. J. Eng. Geol. Environ. 21–31 Special Issue 1.
Boué, A., Lesage, P., Cortés, G., Valette, B., Reyes-Dávila, G., 2015. Real-time eruption forecasting using the material failure Forecast Method with a Bayesian approach. J. Geophys. Res. 120 (4), 2143–2161.
Boyd, J.M., Hinds, D.V., Moy, D., Rogers, C., 1973. Two simple devices for monitoring movements in rock slopes. Q. J. Eng. Geol. Hydrogeol. 6 (3–4), 295–302.
Bozzano, F., Cipriani, I., Mazzanti, P., Prestininzi, A., 2014. A field experiment for calibrating landslide time-of-failure prediction functions. Int. J. Rock Mech. Min. Sci. 67, 69–77.
Brawner, C.O., Stacey, P.F., 1979. Hogarth Pit slope failure, Ontario, Canada. In: Rockslides and Avalanches. vol. 2. Elsevier, Amsterdam, The Netherlands, pp. 691–707. https://doi.org/10.1016/B978-0-444-41508-0.50029-6.
Brown, I., Hittinger, M., Goodman, R., 1980. Finite element study of the Nevis Bluff (New Zealand) rock slope failure. Rock Mech. Rock. Eng. 12, 231–245.
Brox, D., Newcomen, W., 2003. Utilizing strain criteria to predict highwall stability performance. In: Proceedings of the 10th ISRM Congress, Sandton, South Africa.
Brunetti, M.T., Peruccacci, S., Rossi, M., Luciani, S., Valigi, D., Guzzetti, F., 2010. Rainfall thresholds for the possible occurrence of landslides in Italy. Nat. Hazards Earth Syst. Sci. 10 (3), 447–458.
Bui, D.T., Tuan, T.A., Klempe, H., Pradhan, B., Revhaug, I., 2016. Spatial prediction models for shallow landslide hazards: a comparative assessment of the efficacy of support vector machines, artificial neural networks, kernel logistic regression, and logistic model tree. Landslides 13 (2), 361–378.
Cabrejo, A., Harries, N., 2012. Effective Slope Monitoring for Open Cut Coal Mines. Available online at. www.acarp.com.au/abstracts.aspx?RepId=C17023.
Cao, Y., Yin, K., Alexander, D.E., Zhou, C., 2016. Using an extreme learning machine to predict the displacement of step-like landslides in relation to controlling factors. Landslides 13 (4), 725–736.
Carlà, T., Intrieri, E., Di Traglia, F., Casagli, N., 2016. A statistical-based approach for determining the intensity of unrest phases at Stromboli volcano (Southern Italy) using one-step-ahead forecasts of displacement time series. Nat. Haz. 84 (1), 669–683.
Carlà, T., Farina, P., Intrieri, E., Botsialas, K., Casagli, N., 2017a. On the monitoring and early-warning of brittle slope failures in hard rock masses: examples from an open-pit mine. Eng. Geol. 228, 71–81.
Carlà, T., Intrieri, E., Di Traglia, F., Nolesini, T., Gigli, G., Casagli, N., 2017b. Guidelines on the use of inverse velocity method as a tool for setting alarm thresholds and forecasting landslides and structure collapses. Landslides 14 (2), 517–534.
Carlà, T., Intrieri, E., Farina, P., Casagli, N., 2017c. A new method to identify impending failure in rock slopes. Int. J. Rock Mech. Min. Sci. 93, 76–81.
Carlà, T., Macciotta, R., Hendry, M.T., Martin, C.D., Edwards, T., Evans, T., Farina, P., Intrieri, E., Casagli, N., 2017d. Displacement of a landslide retaining wall and application of an enhanced failure forecasting approach. Landslides 15 (3), 489–505.
Carlà, T., Farina, P., Intrieri, E., Ketizmen, H., Casagli, N., 2018. Integration of ground-based radar and satellite InSAR data for the analysis of an unexpected slope failure in an open-pit mine. Eng. Geol. 235, 39–52.
Casagli, N., Tibaldi, A., Merri, A., Del Ventisette, C., Apuani, T., Guerri, L., Fortuny-Guasch, J., Tarchi, D., 2009. Deformation of Stromboli Volcano (Italy) during the 2007 eruption revealed by radar interferometry, numerical modelling and structural geological field data. J. Volcanol. Geotherm. Res. 182 (3–4), 182–200.
Casagli, N., Frodella, W., Morelli, S., Tofani, V., Ciampalini, A., Intrieri, E., Raspini, F., Rossi, G., Tanteri, L., Lu, P., 2017. Spaceborne, UAV and ground-based remote sensing techniques for landslide mapping, monitoring and early warning. Geoenviron. Dis. 4, 9.
Charles, R., 1958. The static fatigue of glass. J. Appl. Phys. 29, 1549–1560.
Chen, H., Lee, C.F., 2003. A dynamic model for rainfall-induced landslides on natural slopes. Geomorphology 51 (4), 269–288.

Chen, H., Zeng, Z., 2012. Deformation prediction of landslide based on improved back-propagation neural network. Cogn. Comput. 5 (1), 56–62.

Chousianitis, K., Del Gaudio, V., Kalogeras, I., Ganas, A., 2014. Predictive model of Arias intensity and Newmark displacement for regional scale evaluation of earthquake-induced landslide hazard in Greece. Soil Dyn. Earthq. Eng. 65, 11–19.

Corcoran, J., Davies, C.M., 2018. Monitoring power-law creep using the failure Forecast Method. Int. J. Mech. Sci. 140, 179–188.

Cornelius, R.R., Scott, P.A., 1993. A materials failure relation of accelerating creep as empirical description of damage accumulation. Rock Mech. Rock. Eng. 26, 233–252.

Cornelius, R., Voight, B., 1994. Seismological aspects of the 1989–1990 eruption at Redoubt Volcano, Alaska: the materials Failure Forecast Method (FFM) with RSAM and SSAM seismic data. J. Volcanol. Geotherm. Res. 62, 469–498.

Cornelius, R.R., Voight, B., 1995. Graphical and PC-software analysis of volcano eruption precursors according to the materials failure forecast method (FFM). J. Volcanol. Geotherm. Res. 64, 295–320.

Corominas, J., Moya, J., Ledesma, A., Lloret, A., Gill, J., 2005. Prediction of ground displacements and velocities from groundwater level changes at the Vallcebre landslide (Eastern Pyrenees, Spain). Landslides 2 (2), 83–96.

Crosta, G.B., Agliardi, F., 2002. How to obtain alert velocity thresholds for large rock-slides. Phys. Chem. Earth, Parts A/B/C 27 (36), 1557–1565.

Crosta, G.B., Agliardi, F., 2003. Failure forecast for large rock slides by surface displacement measurements. Can. Geotech. J. 40 (1), 176–191.

Cruden, D.M., Masoumzadeh, S., 1987. Accelerating creep of the slopes of a coal mine. Rock Mech. Rock. Eng. 20, 123–135.

De Joode, A., Van Steijn, H., 2003. PROMOTOR-df: A GIS-based simulation model for debris-flow hazard prediction. In: Rickenmann, D., Chen, Ch.-L. (Eds.), Debris-Flow Hazards Mitigation: Mechanics, Prediction, and Assessment. Mill Press, Rotterdam, pp. 1173–1184.

De la Cruz-Reyna, S., Reyes-Dávila, G.A., 2001. A model to describe precursory material-failure phenomena: applications to short-term forecasting at Colima volcano, Mexico. Bull. Volcanol. 63 (5), 297–308.

DiBiagio, E., Kjekstad, O., 2007. Early warning, instrumentation and monitoring landslides. In: 2nd Regional Training Course, RECLAIM II, Phuket, Thailand, 29th January–2nd February 2007.

Dick, G.J., Eberhardt, E., Cabrejo-Liévano, A.G., Stead, D., Rose, N.D., 2015. Development of an early-warning time-of-failure analysis methodology for open-pit mine slopes utilizing ground-based slope stability radar monitoring data. Can. Geotech. J. 52 (4), 515–529.

Dietrich, W., Montgomery, D., 1998. Shalstab: A digital terrain model for mapping shallow landslide potential. In: NCASI (National Council of the Paper Industry for Air and Stream Improvement) Technical Report.

Dok, A., Fukuoka, H., Katsumi, T., Inui, T., 2011. Tertiary creep reproduction in back-pressure-controlled ring shear test to understand the mechanism and final failure time of fainfall-induced landslides. In: Annuals of Disas. Prev. Res. Inst. Kyoto Univ. (No. 54 B.).

Du, W., Wang, G., 2016. A one-step Newmark displacement model for probabilistic seismic slope displacement hazard analysis. Eng. Geol. 205, 12–23.

Du, J., Yin, K., Lacasse, S., 2013. Displacement prediction in colluvial landslides, three Gorges Reservoir, China. Landslides 10 (2), 203–218.

Dusseault, M.B., Fordham, C.J., 1993. Time-dependent behavior of rocks. In: Book chapter 6 in Rock Testing and Site Characterization, pp. 119–149 Pergamon.

Eberhardt, E., 2008. Twenty-ninth Canadian Geotechnical Colloquium: the role of advanced numerical methods and geotechnical field measurements in understanding complex deep-seated rock slope failure mechanisms. Can. Geotech. J. 45 (4), 484–510.

Eberhardt, E., Watson, A.D., Loew, S., 2008. Improving the interpretation of slope monitoring and early warning data through better understanding of complex deep-seated landslide failure mechanisms. In: Proceedings of the 10th International Symposium on Landslides, pp. 39–51.

Eberhart, R., Kennedy, J., 1995. A new optimizer using particle swarm theory. In: Proceedings of the 6th International Symposium on Micro Machine and Human Science, Nagoya, Japan, pp. 39–43.

Efron, B., 1979. Bootstrap methods: Another look at the jackknife. In: Kotz, S., Johnson, N.L. (Eds.), Breakthroughs in Statistics. Springer Series in Statistics (Perspectives in Statistics). Springer, New York, NY.

Federico, A., Popescu, M., Murianni, A., 2015. Temporal prediction of landslide occurrence: a possibility or a challenge? Ital. J. Eng. Geol. Env. 1, 41–60.

Fell, R., 1994. Landslide risk assessment and acceptable risk. Can. Geotech. J. 31, 261–272.

Fell, R., Corominas, J., Bonnard, C., Cascini, L., Leroi, E., Savage, W.Z., 2008. Guidelines for landslide susceptibility, hazard and risk zoning for land use planning. Eng. Geol. 102 (3–4), 85–98.

Feng, X.-T., Zhao, H., Li, S., 2004. Modeling non-linear displacement time series of geo-materials using evolutionary support vector machines. Int. J. Rock Mech. Min. Sci. 41 (7), 1087–1107.

Fletcher, L., Hungr, O., Evans, S.G., 2002. Contrasting failure behaviour of two large landslides in clay and silt. Can. Geotech. J. 39 (1), 46–62.

Froude, M.J., Petley, D.N., 2018. Global fatal landslide occurrence from 2004 to 2016. Nat. Hazards Earth Syst. Sci. 18, 2161–2181.

Fukui, K., Okubo, S., 1997. Life expectancy and tertiary creep for rock. In: Proceedings of the Fall Meeting Mining and Minerals Processing Institute of Japan, pp. 91–94 (in Japanese).

Fukuzono, T., 1984. A method for predicting the failure time of a sandy soil slope using the inverse number of velocity. Proceedings of the 23rd Meeting of Japan Landslide Society 80–81 (in Japanese).

Fukuzono, T., 1985a. A new method for predicting the failure time of a slope failure. In:

Proceedings of the 4th International Conference and Field Workshop on Landslides, Tokyo (Japan), pp. 145–150.

Fukuzono, T., 1985b. A method to predict the time of slope failure caused by rainfall using the inverse number of velocity of surface displacement. J. Jap. Landslide Soc. 22, 8–13.

Fukuzono, T., 1990. Recent studies on time prediction of slope failure. Landslide News 4, 9–12.

Fukuzono, T., Terashima, H., 1982. Experimental study of the process of failure in co-hesive soil slope caused by rainfall. Nat. Disaster Res. Rep. NRCDP 29, 103–122 (in Japanese).

Gao, W., Feng, X., 2004. Study on displacement prediction of landslide based on Grey System and Evolutionary Neural Network. In: Proceedings of the 10th International Conference on Enhancement and Promotion of Computational Methods in Engineering and Science (EPMESC X), 21–23 August 2006, Sanya, Hainan (China), pp. 890–894.

Gariano, S.L., Guzzetti, F., 2016. Landslides in a changing climate. Earth Sci. Rev. 162, 227–252.

Geopraevent, A.G., 2012. Rockfall monitoring in Preonzo May 2012. Available online at: https://www.geopraevent.ch/project/interferometric-radar-measurements-preonzoti/?lang=en (Last access on January 29th, 2018).

Gigli, G., Fanti, R., Canuti, P., Casagli, N., 2011. Integration of advanced monitoring and numerical modeling techniques for the complete risk scenario analysis of rockslides: the case of Mt. Beni (Florence, Italy). Eng. Geol. 120 (1–4), 48–59.

Gigli, G., Intrieri, E., Lombardi, L., Nocentini, M., Frodella, W., Balducci, M., Venanti, L., Casagli, N., 2014. Event scenario analysis for the design of rockslide counter-measures. J. Mt. Sci. 11 (6), 1521–1530.

Glastonbury, J., Fell, R., 2002. Report on the analysis of the deformation behaviour of excavated rock slopes. In: UNICIV Report No. R-406. The University of New South Wales, Sydney, Australia.

Gregersen, O., 1981. The quick clay landslide in Rissa, Norway. In: Proceedings of the 10th International Conference on Soil Mechanics and Foundation Engineering, Stocholm. vol. 3. pp. 421–426.

Guzzetti, F., Peruccacci, S., Rossi, M., Stark, C.P., 2007. Rainfall thresholds for the initiation of landslides in central and southern Europe. Meteorog. Atmos. Phys. 98, 239–267.

Hao, S.W., Rong, F., Ming-Fu, L., Wang, H.Y., Xia, M.F., Fu-Jiu, K., Bai, Y.L., 2013. Power-law singularity as a possible catastrophe warning observed in rock experiments. Int. J. Rock Mech. Min. Sci. 60, 253–262.

Hao, S.W., Zhang, B.J., Tian, J.F., Elsworth, D., 2014. Predicting time-to-failure in rock extrapolated from secondary creep. J. Geophys. Res. Solid Earth 119, 1942–1953.

Hao, S.W., Liu, C., Lu, C.S., Elsworth, D., 2016. A relation to predict the failure of materials and potential application to volcanic eruptions and landslides. Sci. Rep. 6, 27877.

Hao, S., Yang, H., Elsworth, D., 2017. An accelerating precursor to predict "time-to-failure" in creep and volcanic eruptions. J. Volcanol. Geotherm. Res. 343, 252–262.

Haque, U., Blum, P., Da Silva, P.F., Andersen, P., Pilz, J., Chalov, S.R., Malet, J.-P., Jemec Auflič, M., Andres, N., Poyiadji, E., Lamas, P.C., Zhang, W., Peshevski, I., Pétursson, H.G., Kurt, T., Dobrev, N., García-Davalillo, J.C., Halkia, M., Ferri, S., Gaprindashvili, G., Engström, J., Keellings, D., 2016. Fatal landslides in Europe. Landslides 13 (6), 1545–1554.

Harries, N., Noon, D., Rowley, K., 2006. Case studies of slope stability radar used in open cut mines. In: Stability of Rock Slopes in Open Pit Mining and Civil Engineering Situations, Southern African Institute of Mining and Metallurgy Symposium Series S44, Cape Town, South Africa, pp. 335–342.

Hayashi, S., Komamura, F., Park, B., Yamamori, T., 1988. On the forecast of time to failure of slope—approximate forecast in the early period of the tertiary creep. J. Jpn. Landslides Soc. 25 (3), 11–16.

Heap, M.J., Baud, P., Meredith, P.G., Vinciguerra, S., Bell, A.F., Main, I.G., 2011. Brittle creep in basalt and its application to time-dependent volcano deformation. Earth Plan. Sci. Lett. 307 (1–2), 71–82.

Heim, A., 1932. Bergsturz und Menschenleben. Fretz & Wasmuth Verlag, Zurich, pp. 218.

Huang, G.-B., Zhou, H., Ding, X., Zhang, R., 2012. Extreme learning machine for regression and multiclass classification. IEEE Trans. Syst. Man Cybern. B 42 (2), 513–529.

Hungr, O., Kent, A., 1995. Coal mine waste dump failures in British Columbia, Canada. Landslide News 9, 26–28.

Hutchinson, J.N., 1987. Mechanisms producing large displacements in landslides on pre-existing shears. Mem. Geol. Soc. China 9, 175–200.

Hutchinson, J.N., 2001. Landslide risk—to know, to foresee, to prevent. Geol. Tecn. Ambient. 9, 3–24.

Intrieri, E., Gigli, G., 2016. Landslide forecasting and factors influencing predictability. Nat. Haz. Earth Syst. Sci. 16 (12), 2501–2510.

Intrieri, E., Gigli, G., Mugnai, F., Fanti, R., Casagli, N., 2012. Design and implementation of a landslide Early Warning System. Eng. Geol. 147–148, 124–136.

Intrieri, E., Gigli, G., Casagli, N., Nadim, F., 2013. Brief communication: Landslide early warning system: Toolbox and general concepts. Nat. Haz. Earth Syst. Sci. 13, 85–90.

Intrieri, E., Raspini, F., Fumagalli, A., Lu, P., Del Conte, S., Farina, P., Allievi, J., Ferretti, A., Casagli, N., 2018a. The Maoxian landslide as seen from space: detecting precursors of failure with Sentinel-1 data. Landslides 15 (1), 123–133.

Intrieri, E., Gigli, G., Gracchi, T., Nocentini, M., Lombardi, L., Mugnai, F., Frodella, W., Bertolini, G., Carnevale, E., Favalli, M., Fornaciai, A., Marturià Alavedra, J., Mucchi, L., Nannipieri, L., Rodriguez-Lloveras, X., Pizziolo, M., Schina, R., Trippi, F., Casagli, N., 2018b. Application of an ultra-wide band sensor-free wireless network for ground monitoring. Eng. Geol. 238, 1–14.

Iovine, G., Petrucci, O., Rizzo, V., Tansi, C., 2006. The March 7th 2005 Cavallerizzo (Cerzeto) landslide in Calabria - Southern Italy. In: Proceedings of the 10th IAEG

Congress, Nottingham, Great Britain. Geological Society of London, pp. 12 (paper n. 785).

Jäggli, M., 1928. Il cataclisma tellurico al Motto d'Arbino. In: Ticino 5. vol. 11. pp. 161–164.

Jurich, D.M., Miller, R.J., 1987. Acoustic monitoring of landslides. In: Transportation Research Record No. 1119.

Kayesa, G., 2006. Prediction of slope failure at Letlhakane mine with the geomos slope monitoring system. In: Proceedings of the International Symposium on Stability of Rock Slopes in Open Pit Mining and Civil Engineering, pp. 605–622.

Kennedy, B.A., Niermeyer, K.E., 1970. Slope monitoring systems used in the prediction of a major slope failure at the Chuquicamata Mine, Chile. In: Proceedings of Planning Open Pit Mines, Johannesburg, 29 August – 4 September 1970, Cape Town, pp. 215–225.

Keqiang, H., Sijing, W., 2006. Double parameter threshold and its formation mechanism of the colluvial landslide: Xintan landslide, China. Environ. Geol. 49, 696–707.

Kilburn, C.R.J., 2003. Multiscale fracturing as a key to forecasting volcanic eruptions. J. Volcanol. Geotherm. Res. 125, 271–289.

Kilburn, C., 2012. Precursory deformation and fracture before brittle rock failure and potential application to volcanic unrest. J. Geophys. Res. 117, B02211.

Kilburn, C.R.J., Petley, D.N., 2003. Forecasting giant, catastrophic slope collapse: lessons from Vajont, northern Italy. Geomorphology 54 (1–2), 21–32.

Kilburn, C.R.J., Voight, B., 1998. Slow rock fracture as eruption precursor at Soufriere Hills volcano, Montserrat. Geophys. Res. Lett. 25, 3665–3668.

Kim, T.H., Cruden, D.M., Martin, D., Froese, C.R., Morgan, A.J., 2010. Landslide movements and their characteristic, Town of Peace River, Alberta. In: Proceedings of the 63rd Canadian Geotechnical Conference and 6th Canadian Permafrost Conference, Calgary, Alberta.

Klose, M., Maurischat, P., Damm, B., 2015. Landslide impacts in Germany: a historical and socioeconomic perspective. Landslides 13 (1), 183–199.

Kothari, U.C., Momayez, M., 2018. New approaches to monitoring, analyzing and predicting slope instabilities. J. Geol. Min. Res. 10 (1), 1–14.

Krähenbühl, R., 2006. Der Felssturz, der sich auf die Stunde genau ankündigte. Bull. Angew. Geol. 11 (1), 49–63.

Krkač, M., Špoljarić, D., Bernat, S., Arbanas, S.M., 2017. Method for prediction of landslide movements based on random forests. Landslides 14 (3), 947–960.

Lacasse, S., Nadim, F., 2008. Landslide risk assessment and mitigation strategy. In: Sassa, K., Canuti, P. (Eds.), Landslides – Disaster Risk Reduction. Springer Verlag, Berlin Heidelberg, pp. 31–61.

Lambe, T.W., 1973. Predictions in soil engineering. Géotechnique 23 (2), 151–202.

Lavallée, Y., Meredith, P.G., Dingwell, D.B., Hess, K.U., Wassermann, J., Cordonnier, B., Gerik, A., Kruhl, J.H., 2008. Seismogenic lavas and explosive eruption forecasting. Nature 453, 507–510.

Le Breton, M., Baillet, L., Larose, E., Rey, E., Benech, P., Jongmans, D., Guyoton, F., Jaboyedoff, M., 2019. Passive radio-frequency identification ranging, a dense and weather-robust technique for landslide displacement monitoring. Eng. Geol. 1–10.

Le, Q.H., Van Nguyen, T.H., Do, M.D., Le, T.C.H., Nguyen, H.K., Luu, T.B., 2018. TXT-tool 1.084-3.1: Landslide Susceptibility Mapping at a Regional Scale in Vietnam. In: Landslide Dynamics: ISDR-ICL Landslide Interactive Teaching Tools. Springer, Cham, pp. 161–174.

Li, T., Chen, M., Wang, L., Zhou, Y., 1996. Time prediction of landslides using Verhulst inverse-function model. In: Proceedings of 7th international symposium on landslides, Trondheim, pp. 1289–1293.

Li, X., Kong, J., Wang, Z., 2012. Landslide displacement prediction based on combining method with optimal weight. Nat. Haz. 61 (2), 635–646.

Lian, C., Zeng, Z., Yao, W., Tang, H., 2015. Multiple neural networks switched prediction for landslide displacement. Eng. Geol. 186, 91–99.

Liu, Z., Shao, J., Xu, W., Chen, H., Shi, C., 2014. Comparison on landslide nonlinear displacement analysis and prediction with computational intelligence approaches. Landslides 11 (5), 889–896.

Lockner, D., 1993. Room temperature creep in saturated granite. J. Geophys. Res. 98, 475–487.

Loew, S., Gschwind, S., Gischig, V., Keller-Signer, A., Valenti, G., 2017. Monitoring and early warning of the 2012 Preonzo catastrophic rockslope failure. Landslides 14 (1), 141–154.

Lombardi, L., Nocentini, M., Frodella, W., Nolesini, T., Bardi, F., Intrieri, E., Carlà, T., Solari, L., Dotta, G., Ferrigno, F., Casagli, N., 2017. The Calatabiano landslide (Southern Italy): preliminary GB-InSAR monitoring data and remote 3D mapping. Landslides 14 (2), 685–696.

Lu, P., Rosenbaum, M.S., 2003. Artificial neural networks and grey systems for the prediction of slope stability. Nat. Haz. 30 (3), 383–398.

MacRae, A.M.R., 1982. Case histories of deformation measurements in Canadian surface mines. In: Proceedings of the 4th Canadian Symposium on Mining, Surveying and Deformation Measurements, Ottawa, Canada, pp. 255–278.

Main, I.G., 2000. A damage mechanics model for power-law creep and earthquake aftershock and foreshock sequences. Geophys. J. Int. 142, 151–161.

Manconi, A., Giordan, D., 2016. Landslide failure forecast in near-real-time. Geomat. Nat. Haz. Risk 7 (2), 639–648.

Mazzanti, P., Bozzano, F., Cipriani, I., Prestininzi, A., 2015. New insights into the temporal prediction of landslides by a terrestrial SAR interferometry monitoring case study. Landslides 12 (1), 55–68.

McDougall, S., 2016. 2014 Canadian Geotechnical Colloquium: Landslide runout analysis—current practice and challenges. Can. Geotech. J 54 (5), 605–620.

Miao, F., Wu, Y., Xie, Y., Li, Y., 2018. Prediction of landslide displacement with step-like behavior based on multialgorithm optimization and a support vector regression model. Landslides 15 (3), 475–488.

Minamitani, T., 2007. An Experimental Study on the Parameter Affecting Tertiary Creep Deformation of Soils (Master thesis). DPRI, Kyoto University, Japan.

Mucchi, M., Jayousi, S., Martinelli, A., Caputo, S., Intrieri, E., Gigli, G., Gracchi, T., Mugnai, F., Favalli, M., Fornaciai, A., Nannipieri, L., 2018. Flexible wireless sensor network based on ultra-wide band technology for ground instability monitoring. Sensors 18 (9), 2948. https://doi.org/10.3390/s18092948.

Mufundirwa, A., Fujii, Y., Kodama, J., 2010. A new practical method for prediction of geomechanical failure-time. Int. J. Rock Mech. Min. Sci. 47 (7), 1079–1090.

Neaupane, K.M., Achet, S.H., 2004. Use of backpropagation neural network for landslide monitoring: a case study in the higher Himalaya. Eng. Geol. 74 (3–4), 213–226.

Newcomen, W., Dick, G., 2015. An update to strain-based pit wall failure prediction method and a justification for slope monitoring. In: Proceedings of Slope Stability 2015 – International Symposium on Slope Stability in Open Pit Mining and Civil Engineering, 12–14 October 2015, Cape Town, South Africa, pp. 139–150.

Noverraz, F., Bonnard, C., 1992. Le glissement rapide de La Chenaula. In: Internationales Symposium INTERPRAEVENT 1992 – Bern, pp. 65–76 (in French).

Osasan, K.S., Stacey, T.R., 2014. Automatic prediction of time to failure of open pit mine slopes based on radar monitoring and inverse velocity method. Int. J. Min. Sci. Tech. 24 (2), 275–280.

Petley, D.N., 2004. The evolution of slope failures: mechanisms of rupture propagation. Nat. Haz. Earth Syst. Sci. 4, 147–152.

Petley, D.N., 2012. Global patterns of loss of life from landslides. Geology 40 (10), 927–930.

Petley, D.N., Bulmer, M.H., Murphy, W., 2002. Patterns of movement in rotational and translational landslide. Geology 30, 719–722.

Petley, D.N., Dunning, S.A., Rosser, N.J., 2005a. The analysis of global landslide risk through the creation of a database of worldwide landslide fatalities. In: Landslide Risk Management. Balkema, Amsterdam, pp. 367–374.

Petley, D.N., Higuchi, T., Petley, D.J., Bulmer, M.H., Carey, J., 2005b. Development of progressive landslide failure in cohesive materials. Geology 33 (3), 201–204.

Petley, D.N., Mantovani, F., Bulmer, M.H., Zannoni, A., 2005c. The use of surface monitoring data for the interpretation of landslide movement patterns. Geomorphology 66 (1–4), 133–147.

Piciullo, L., Calvello, M., Cepeda, J., 2018. Territorial early warning systems for rainfall-induced landslides. Earth Sci. Rev. 179, 228–247.

Ponziani, F., Pandolfo, C., Stelluti, M., Berni, N., Brocca, L., Moramarco, T., 2012. Assessment of rainfall thresholds and soil moisture modeling for operational hydrogeological risk prevention in the Umbria region (central Italy). Landslides 9 (2), 229–237.

Randall, J.W., 2007. Regression models for estimating coseismic landslide displacement. Eng. Geol. 91 (2–4), 209–218.

Raspini, F., Bianchini, S., Ciampalini, A., Del Soldato, M., Solari, L., Novali, F., Del Conte, S., Rucci, A., Ferretti, A., Casagli, N., 2018. Continuous, semi-automatic monitoring of ground deformation using Sentinel-1 satellites. Sci. Rep. 8, 7253.

Read, J., Stacey, P., 2009. Guidelines for open pit slope design. CSIRO Publishing, Collingwood, Australia.

Rickenmann, D., 2005. Runout prediction methods. In: Debris-Flow Hazards and Related Phenomena. Springer Praxis Books. Springer, Berlin, Heidelberg, pp. 305–324.

Rose, N.D., Hungr, O., 2007. Forecasting potential rock slope failure in open pit mines using the inverse velocity method. Int. J. Rock Mech. Min. Sci. 44 (2), 308–320.

Rosser, N., Lim, M., Petley, D., Dunning, S., Allison, R., 2007. Patterns of precursory rockfall prior to slope failure. J. Geophys. Res. 112, F04014.

Rossi, G., Catani, F., Leoni, L., Segoni, S., Tofani, V., 2013. HIRESSS: a physically based slope stability simulator for HPC applications. Nat. Hazards Earth Syst. Sci. 13 (1), 151–166.

Royán, M.J., Abellán, A., Vilaplana, J.M., 2015. Progressive failure leading to the 3 December 2013 rockfall at Puigcercós scarp (Catalonia, Spain). Landslides 12 (3), 585–595.

Saito, M., 1965. Forecasting the time of occurrence of slope failure. In: Proceeding of the 6th International Conference on Soil Mechanics and Foundation Engineering, Montreal. vol. 2. pp. 537–541.

Saito, M., 1969. Forecasting Time of Slope failure by Tertiary Creep. In: Proceedings of the 7th International Conference on Soil Mechanics and Foundation Engineering, Mexico City. vol. 2. pp. 677–683.

Saito, M., Uezawa, M., 1961. Failure of soil due to creep. In: Proceedings of the 5th International Conference on Soil Mechanics and Foundation Engineering, Mexico City. vol. 1. pp. 315–318.

Salciarini, D., Godt, J., Savage, W., Conversini, P., Baum, R., Michael, J., 2006. Modeling regional initiation of rainfall-induced shallow landslides in the eastern umbria region of central Italy. Landslides 3, 181–194.

Sättele, M., Krautblatter, M., Bründl, M., Straub, D., 2016. Forecasting rock slope failure: how reliable and effective are warning systems? Landslides 13 (4), 737–750.

Scholz, C., 1972. Static fatigue of quartz. J. Geophys. Res. 77, 2104–2114.

Schumm, S.A., Chorley, R.J., 1964. The fall of threatening rock. Am. J. Sci. 262, 1041–1054.

Schuster, R.L., Highland, L., 2001. Socioeconomic and environmental impacts of landslides in the western hemisphere. In: US Geological Survey Open-File Report 01–0276.

Segalini, A., Valletta, A., Carri, A., 2018. Landslide time-of-failure forecast and alert threshold assessment: a generalized criterion. Eng. Geol. 245, 72–80.

Shieh, C.L., Chen, Y.S., Tsai, Y.J., Wu, J.H., 2009. Variability in rainfall threshold for debris flow after the Chi-Chi earthquake in central Taiwan, China. Int. J. Sediment. Res. 24 (2), 177–188.

Simoni, S., Zanotti, F., Bertoldi, G., Rigon, R., 2008. Modelling theprobability of occurrence of shallow landslides and channelized debris flows using geotop-fs. Hydrol. Process. 22, 532–545.

Smith, R., Kilburn, C.R.J., 2010. Forecasting eruptions after long repose intervals from

accelerating rates of rock fracture: the June 1991 eruption of Mount Pinatubo, Philippines. J. Volcanol. Geotherm. Res. 191, 129–136.

Smith, R., Sammonds, P.R., Kilburn, C.R.J., 2009. Fracturing of volcanic systems: Experimental insights into pre-eruptive conditions. Earth Planet. Sci. Lett. 280, 211–219.

Sornette, D., Helmstetter, A., Andersen, J.V., Gluzman, S., Grasso, J.R., Pisarenko, V., 2004. Towards landslide predictions: two case studies. Phys. A Stat. Mech. Appl. 338 (3–4), 605–632.

Stähli, M., Sättele, M., Huggel, C., McArdell, B.W., Lehmann, P., Van Herwijnen, A., Berne, A., Schleiss, M., Ferrari, A., Kos, A., Or, D., Springman, S.M., 2015. Monitoring and prediction in early warning systems for rapid mass movements. Nat. Hazards Earth Syst. Sci. 15 (4), 905–917.

Suwa, H., 1991. Visually observed failure of rock slope in Japan, international newsletter. Landslide News 5, 8–10.

Suwa, H., Mizuno, T., Ishii, T., 2010. Prediction of a landslide and analysis monitoring of slide motion with reference to the 004 Ohto slide in Nara, Japan. Geomorphology 124, 157–163.

Szwedzicki, T., 2003. Rock mass behaviour prior to failure. Int. J. Rock Mech. Min. Sci. 40 (4), 573–584.

Tavenas, F., Leroueil, S., 1981. Creep and failure of slopes in clays. Can. Geotech. J. 18 (1), 106–120.

Terzaghi, K., 1950. Mechanisms of Landslides. Geotechnical Society of America, Berkeley, pp. 83–125.

UNISDR (United Nations International Strategy For Disaster Reduction), 2006. The International Early Warning Programme – The four elements of effective early warning systems – Brochure, Platform for the Promotion of Early Warning. PPEW 4 pp., available at. http://www.unisdr.org/2006/ppew/iewp/IEWP-brochure.pdf.

Urciuoli, G., Picarelli, L., 2008. Interaction between landslides and man-made works. In: Chen (Ed.), Landslides and Engineered Slopes. Taylor & Francis Group, London, pp. 2008.

Van Westen, C.J., Castellanos, E., Kuriakose, S.L., 2008. Spatial data for landslide susceptibility, hazard, and vulnerability assessment: an overview. Eng. Geol. 102 (3–4), 112–131.

Varnes, D.J., 1982. Time-deformation relations in creep to failure of earth materials. In: Proceedings of the 7th Southeast Asia Geotechnical Conference, Hong Kong, pp. 107–130.

Venter, J., Kuzmanovic, A., Wessels, S.D.N., 2013. An evaluation of the CUSUM and inverse velocity methods of failure prediction based on two open pit instabilities in the Pilbara. In: Proceedings of Slope Stability 2013, Australian Centre for Geomechanics, Brisbane, Australia, pp. 1061–1076.

Vilhelm, J., Rudajev, V., Lokajíček, T., Živor, R., 2008. Application of autocorrelation analysis for interpreting acoustic emission in rock. Int. J. Rock Mech. Min. Sci. 45 (7), 1068–1081.

Voight, B., 1988. A method for prediction of volcanic eruption. Nature 332, 125–130.

Voight, B., 1989a. A relation to describe rate-dependent material failure. Science 243, 200–203.

Voight, B., 1989b. Materials science law applies to time forecasts of slope failure. Landslide News 3, 8–11.

Voight, B., Kennedy, B.A., 1979. Slope failure of 1967-1969, Chuquicamata mine, Chile. In: Developments of Geotechnical Engineering. vol. 14. pp. 595–632 part B.

Wyllie, D.C., Munn, F.J., 1979. The use of movement monitoring to minimize production losses due to pit slope failures. In: Proceedings of the 1st International Symposium on Stability in Coal Mining. Miller Freeman San Francisco, Vancouver, Canada, pp. 75–94.

Xu, Q., Yuan, Y., Zeng, Y.P., Hack, R., 2011. Some new pre-warning criteria for creep slope failure. Sci. China Tech. Sci. 54 (1), 210–220.

Yao, W., Zeng, Z., Lian, C., Tang, H., 2015. Training enhanced reservoir computing predictor for landslide displacement. Eng. Geol. 188, 101–109.

Yoshida, T., Yachi, M., 1984. On the velocity of landslide. In: Proceedings of the 23rd Meeting of Japan Landslide Society, pp. 136–139 (in Japanese).

Zavodni, A.M., 2001. Time-dependent movements of open pit slope. In: Slope Stability in Surface Mining, SME Proceedings, Denver, Colorado, pp. 81–87.

Zavodni, Z.M., Broadbent, C.D., 1978. Slope failure kinematics. Bull. Can. Inst. Min. 73, 69–74.

Zhou, C., Yin, K., Cao, Y., Ahmed, B., 2016. Application of time series analysis and PSO–SVM model in predicting the Bazimen landslide in the Three Gorges Reservoir, China. Eng. Geol. 204, 108–120.

Zhou, C., Yin, K., Cao, Y., Intrieri, E., Ahmed, B., Catani, F., 2018. Displacement prediction of step-like landslide by applying a novel kernel extreme learning machine method. Landslides. https://doi.org/10.1007/s10346-018-1022-0.

Zvelebil, J., 1985. Time prediction of a rockfall from a sandstone rock slope. In: Proceedings of the 4th International Symposium on Landslides, Toronto, Canada. 3. pp. 93–96.

Zvelebil, J., Moser, M., 2001. Monitoring based time-prediction of rock falls: three case-histories. Phys. Chem. Earth Pt. B 26 (2), 159–167.